Evaluation of Turbulent Transport and Dissipation Closures in Second-Order Modeling

CHIN-HOH MOENG AND JOHN C. WYNGAARD

National Center for Atmospheric Research, Boulder, Colorado*

(Manuscript received 15 November 1988, in final form 2 March 1989)

ABSTRACT

We show that the turbulence statistics from our $(96)^3$ large-eddy-simulation (LES) studies of a convective boundary layer are in excellent agreement with those from the Deardorff–Willis laboratory convection tank. Using these LES data, we evaluate contemporary parameterizations for turbulent transport and dissipation in second-order closure models of the convective boundary layer. The gradient-diffusion parameterization for turbulent transport fares poorly, due in large part to the direct influence of buoyancy. This leads to poor predictions of the vertical profiles of some turbulence statistics. We also find that the characteristic length scales for the mechanical and thermal dissipation rates typically used in second-order closure models are a factor of 2–3 too small; this leads to underpredictions of turbulence kinetic energy levels. Finally, we find that the flux and variance budgets for conservative scalars are substantially different in top-down and bottom-up diffusion. In order to reproduce these differences accurately, it seems necessary to model the turbulent transport, pressure covariance, and molecular destruction terms differently in top-down and bottom-up diffusion.

1. Introduction

Steadily increasing computer power now allows modelers to use the second-order closure technique with multiple vertical gridpoints to parameterize planetary boundary layer (PBL) turbulence in larger-scale meteorological models. Second-order closure has been used in turbulence calculations since at least the early 1970s. Many of its first applications (e.g., Hanjalic and Launder 1972) were to shear flows; Donaldson (1973) was one of the first to apply it to PBL modeling. The works of later users are summarized in Table 1. (Numerous meteorological models, such as the Klemp–Wilhemson 1978 cloud model, use a simplified version of second-order closure by solving only the turbulence kinetic energy equation; these are not included in Table 1.) Reviews of second-order closure modeling have been done by Mellor and Herring (1973), Lumley and Khajeh-Nouri (1974), Lewellen (1977), Lumley (1978), Zeman (1981), Wyngaard (1982), and Mellor and Yamada (1982).

In PBL applications second-order closure is, in principle, less restrictive than integral (e.g., mixed-layer) modeling and it also provides information on the vertical distribution of turbulence statistics. However, many second-order closures stem from laboratory turbulence data of uncertain relevance to the convective PBL; they were developed in the early 1970s before data from major field programs, laboratory convection tanks, and large-eddy simulation (LES) became available.

Part of the motivation for second-order closure is the hope, expressed by Lumley and Khajeh-Nouri (1974), that "if a crude assumption for second moments predicts first moments adequately, perhaps a crude assumption for third moments will predict second moments adequately." In the mid-1970s, however, some modelers closed at even higher order, by assuming that the fourth moments are jointly Gaussian (e.g., André et al. 1976; Zeman and Lumley 1976). While the predictions of third-order closure have shown good agreement with atmospheric and laboratory tank observations, such models are too complex for practical use in typical large-scale meteorological models.

On the other hand, eddy-diffusivity closure (i.e., K-theory) sometimes gives unrealistic results. Most PBL modelers have chosen intermediate closures, as shown in Table 1. More than two-thirds of the models use the downgradient-diffusion assumption for the third moments whose divergences appear in the second-moment equations. About that fraction of the models diagnoses the turbulent dissipation rates through variances and a specified turbulent length scale; their closure problem is to determine the behavior of this length scale. A few modelers (e.g., Lumley 1970; Wyngaard and Coté 1974) have carried rate equations for the dissipation rates.

There have been indications that a downgradient-diffusion approximation for third moments is invalid

* The National Center for Atmospheric Research is sponsored by the National Science Foundation.

Corresponding author address: Dr. Chin-Hoh Moeng, NCAR/MMM, P.O. Box 3000, Boulder, CO 80307-3000.

TABLE 1. Second-order closure models for the PBL.

Users	Transport closure	Dissipation closure	Applications
Donaldson (1973)	Downgradient diffusion	Diagnostic L^*	Clear PBL
Lewellen and Teske (1973)	Downgradient diffusion	Diagnostic L	Surface layer
Mellor (1973)	Downgradient diffusion	Diagnostic L	Surface layer
Wyngaard and Cote (1974)	Downgradient diffusion	Dissipation Eq.	Clear convective PBL
Mellor and Yamada (1974)	Downgradient diffusion	Diagnostic L	Clear PBL
Wyngaard (1975)	Downgradient diffusion	Dissipation Eq.	Clear stable PBL
Yamada and Mellor (1975)	Downgradient diffusion	Diagnostic L	Clear PBL
Mellor and Durbin (1975)	Downgradient diffusion	Diagnostic L	Ocean boundary layer
Zeman and Lumley (1976)	Buoyancy transport	Dissipation Eq.	Clear convective PBL
Burk (1977)	Downgradient diffusion	Diagnostic L	Clear PBL
Miyakoda and Sirutis (1977)	Downgradient diffusion	Diagnostic L	GCM
Oliver et al. (1978)	Downgradient diffusion	Length-Scale Eq.	Stratus-topped PBL
Brost and Wyngaard (1978)	Ignored	Diagnostic L	Clear stable PBL
Sun and Ogura (1980)	Buoyancy transport	Diagnostic L	Clear convective PBL
Moeng and Arakawa (1980)	Downgradient diffusion	Diagnostic L	Stratus-topped PBL
Klein and Coantic (1981)	Downgradient diffusion	Diagnostic L	Ocean boundary layer
Mailhot and Benoit (1982)	Downgradient diffusion	Prognostic L	Clear PBL
Chen and Cotton (1983)	Buoyant transport	Diagnostic L	Stratus-topped PBL
Therry and Lacarrére (1983)	Buoyant transport	Diagnostic L	Clear PBL
Finger and Schmidt (1986)	Downgradient diffusion	Diagnostic L	Clear PBL
Duynkerke and Driedonks (1987)	Downgradient diffusion	Diag. L & ϵ-eg	Stratus-topped PBL
Wai (1988)	Downgradient diffusion	Diagnostic L	Stratus-topped PBL
Helfand and Labraga (1988)	Downgradient diffusion	Diagnostic L	GCM

* L refers to the dissipation length scale defined in (2.3) and (2.9).

in convective turbulence. Wyngaard (1973) indicated that Kansas data showed positive values of both $\overline{w^3}$ and $\partial\overline{w^2}/\partial z$ in the convective surface layer; hence, the vertical turbulent flux of $\overline{w^2}$ is *upgradient* there. Zeman and Lumley (1976), citing laboratory data, suggested that the downgradient-diffusion model is also inadequate for the vertical flux of total kinetic energy.

In this paper, we will use LES data to get further insight into the downgradient-diffusion closure for third moments and length-scale closures for the turbulent dissipation rates. The LES approach explicitly calculates the large eddies in a turbulent flow field, thus providing three-dimensional data that can be used to study details of the turbulence. Moeng and Wyngaard (1986), using $(40)^3$ LES, studied the maintenance of the scalar-pressure gradient covariance and found that buoyancy and turbulence effects are equally important; they proposed a buoyancy correction to Rotta's (1951) "return-to-isotropy" closure for this term. We postponed the study of turbulent transport and dissipation closures until now, because the higher moments are more sensitive to the numerical resolution of LES, as we show later.

This paper is based on a finer-mesh LES with $(96)^3$ grid points (Moeng and Wyngaard 1988). With such turbulence data, as well as data from direct observations in the lower atmosphere and in laboratory convection tanks, it is now possible to study these closures more systematically than ever before. In this paper, we briefly review the second-order closure technique in section 2. Section 3 presents some second and third-moment statistics from the $(96)^3$ LES, comparisons with the $(40)^3$ LES and with observations, and the LES budgets of turbulence kinetic energy, buoyancy flux, and temperature variance. Closure evaluations, based on our LES data, are given in section 4. Section 5 discusses the implications for second-order closure models.

2. An overview of second-order closure modeling

Second-order closure models often include a prognostic equation for the turbulence kinetic energy $\overline{q^2}/2 = \overline{u^2 + v^2 + w^2}/2$. In the usual notation, the $q^2/2$ equation for a horizontally homogeneous PBL reads

$$\frac{\partial \overline{q^2}/2}{\partial t} = -\frac{\partial \overline{wq^2}/2}{\partial z} - \left(\overline{uw}\frac{\partial U}{\partial z} + \overline{vw}\frac{\partial V}{\partial z}\right) + \beta g\overline{w\theta} - \frac{1}{\rho_0}\frac{\partial \overline{wp}}{\partial z} - \epsilon, \quad (2.1)$$

where U and V are the mean horizontal winds, $\overline{uw}$ and $\overline{vw}$ are the momentum fluxes, βg is the thermal coefficient, $\overline{w\theta}$ is the buoyancy flux, $\overline{wp}$ is the pressure flux, ϵ is the viscous dissipation rate, and the overbar stands for the ensemble average. The terms on the right-hand side represent turbulent transport, shear production, buoyant production, pressure transport, and viscous dissipation, respectively. To solve (2.1), given the mean wind field and the buoyancy and momentum fluxes, we need closure expressions for the turbulent transport, pressure transport, and viscous dissipation terms.

The most commonly used closure for the turbulent

transport term is the downgradient diffusion model (e.g., Donaldson 1973; Mellor and Yamada 1974),

$$\frac{\partial \overline{wq^2}/2}{\partial z} = -\frac{\partial}{\partial z}\left(L_1 q \frac{\partial \overline{q^2}/2}{\partial z}\right), \tag{2.2}$$

where L_1 and $q = (\overline{q^2})^{1/2}$ are length and velocity scales, respectively. The pressure transport term in (2.1) is typically either neglected or implicitly modeled together with the turbulent transport.

Most second-order closure models parameterize viscous dissipation as

$$\epsilon = q^3/L_2, \tag{2.3}$$

where L_2 is another length scale. The basis of this parameterization is that although viscous dissipation is carried out by the smallest eddies, its value is determined by the rate of energy cascade from the energy-containing eddies; hence, it can be expressed in terms of large-eddy properties. Equation (2.3) then results from standard scaling arguments (Tennekes and Lumley 1972).

In convective turbulence, eddy-diffusivity parameterizations for scalar fluxes, e.g., for $\overline{w\theta}$ in (2.1), are not generally valid (e.g., Deardorff 1966). Therefore, second-order closure models usually also include parameterized versions of the scalar-flux and -variance equations; the scalar can be potential temperature θ, or the mixing ratio of water vapor or another conservative species. The scalar-flux equation reads

$$\frac{\partial \overline{wc}}{\partial t} = -\frac{\partial \overline{w^2 c}}{\partial z} - \overline{w^2}\frac{\partial C}{\partial z} + \beta g \overline{c\theta} - \frac{1}{\rho_0}\overline{c\frac{\partial p}{\partial z}}, \tag{2.4}$$

and the variance equation reads

$$\frac{\partial \overline{c^2}}{\partial t} = -\frac{\partial \overline{wc^2}}{\partial z} - 2\overline{wc}\frac{\partial C}{\partial z} - \chi_c, \tag{2.5}$$

where c is the scalar fluctuation, C its mean value, and χ_c its molecular destruction rate. The first two terms on the right-hand sides of (2.4) and (2.5) are the turbulent transport and mean-gradient production. The third and last terms in (2.4) are the buoyant production and pressure covariance. The turbulent transport, pressure covariance, and molecular terms need closure assumptions.

The most common closure for turbulent transport of scalar flux and variance is again the down-gradient diffusion model,

$$\frac{\partial \overline{w^2 c}}{\partial z} = -\frac{\partial}{\partial z}\left(L_3 q \frac{\partial \overline{wc}}{\partial z}\right), \tag{2.6}$$

$$\frac{\partial \overline{wc^2}}{\partial z} = -\frac{\partial}{\partial z}\left(L_4 q \frac{\partial \overline{c^2}}{\partial z}\right), \tag{2.7}$$

where L_3 and L_4 are length scales.

The closure for the pressure covariance is typically an extended version of Rotta's return-to-isotropy hypothesis (Mellor 1973),

$$-\frac{1}{\rho_0}\overline{c\frac{\partial p}{\partial z}} = -q\frac{\overline{wc}}{L_5}, \tag{2.8}$$

where L_5 is another length scale. The scalar variance dissipation is modeled as

$$\chi_c = q\overline{c^2}/L_6, \tag{2.9}$$

where L_6 is a length scale.

Since the six length scales in Eqs. (2.2), (2.3), and (2.6)–(2.9) are representative of the energy-containing turbulence, it might seem reasonable to assume they are proportional to a master length scale L; i.e., $L_i = c_i L$, where c_i, $i = 1, \cdots, 6$, are constants. A commonly used length-scale formula is that of Blackadar (1962):

$$L = \frac{kz}{1 + kz/L_0}, \tag{2.10}$$

where k is the von Karman constant and L_0 is an asymptotic value defined as

$$L_0 = \frac{\alpha_b \int_0^{z_i} qz\,dz}{\int_0^{z_i} q\,dz}, \tag{2.11}$$

where α_b is an empirical constant set to 0.1 by Mellor and Yamada (1974), and z_i the PBL depth.

The closures (2.2), (2.3), and (2.6)–(2.9) were originally developed to model turbulent shear flows, and their adjustable constants were mostly obtained from laboratory data from such flows (e.g., Mellor 1973). Three major deficiencies of these closures have been mentioned in the literature. First, the downgradient transport assumption of (2.2), (2.6), and (2.7) is inadequate in the convective PBL (Wyngaard 1973; Zeman and Lumley 1976; André et al. 1976). The second deficiency relates to the length scales; in their 1982 review paper Mellor and Yamada stated that "the major weakness of all the models probably relates to the turbulent master length scale, and, most important, to the fact that one sets all process scales proportional to a single scale." The third deficiency is the neglect of buoyancy effects on the pressure-scalar covariance closure in (2.8); this was studied by Moeng and Wyngaard (1986). We will consider the first two points in more detail in section 4.

3. Overall statistics from LES

The statistics shown here are from $(96)^3$, wave-cutoff filtered simulations over a 5 km × 5 km × 2 km numerical domain (Moeng and Wyngaard 1988). They are averaged over the horizontal plane and over about three large-eddy-turnover-times z_i/w_*, where $w_* = (\beta g \overline{w\theta}_0 z_i)^{1/3} = \overline{w\theta}_0 = w_*\theta_*$ is the surface buoyancy flux. The simulated PBL has $w_* \approx 2$ m s^{-1}, $u_* \approx 0.6$ m s^{-1}, $z_i \approx 1000$ m, $\overline{w\theta}_0 = 0.24$ K m s^{-1}. Figure 1

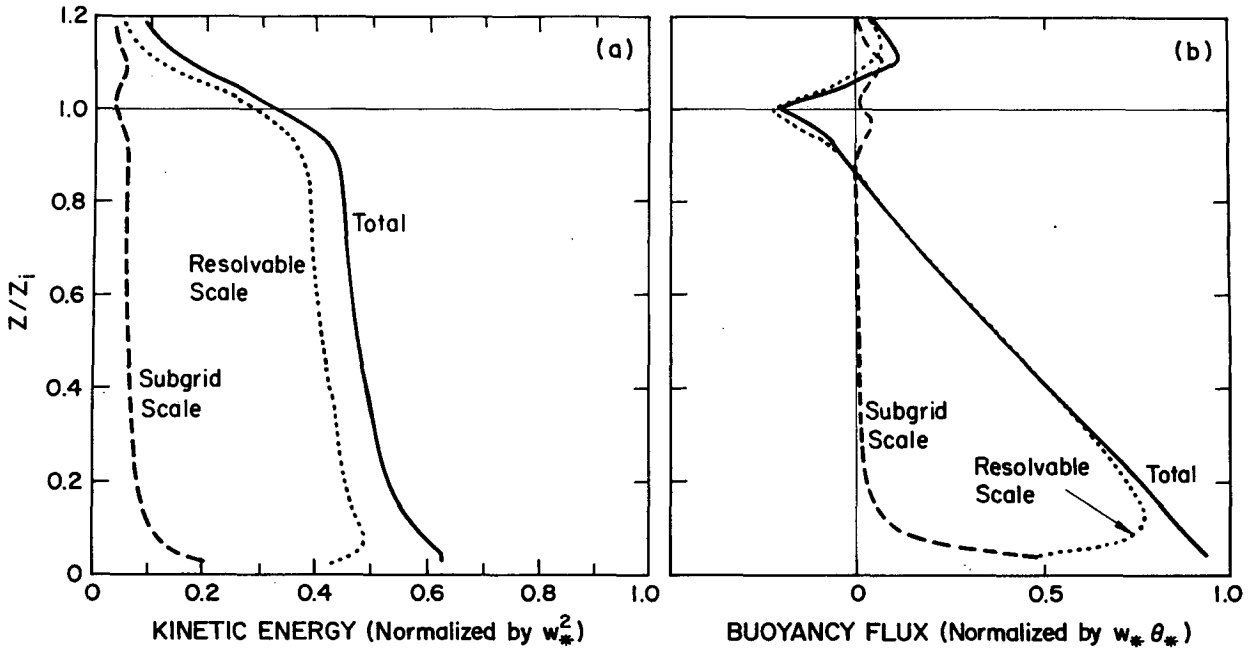

FIG. 1. Vertical distributions of (a) turbulence kinetic energy and (b) buoyancy flux from the $(96)^3$ LES.

shows the resolvable-scale and subgrid-scale kinetic energy and buoyancy flux. Above the surface layer, the subgrid scales contribute less than 12% of the total kinetic energy and support a negligible amount of buoyancy flux.

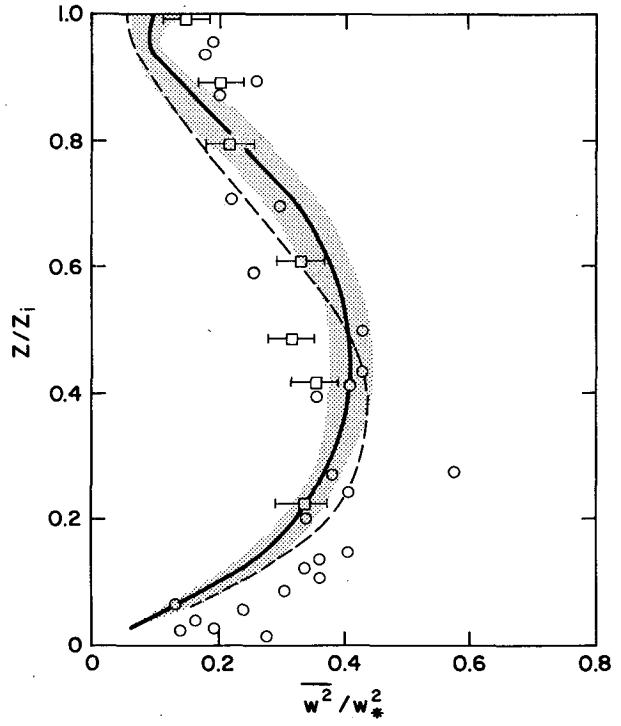

FIG. 2. Vertical velocity variance from the $(96)^3$ LES (solid curve), the $(40)^3$ LES (dashed curve), AMTEX (circles) and convection tank experiments (squares).

Figure 2 shows the vertical velocity variance; the shaded area covers all the vertical profiles at each recorded time, and hence indicates the sampling error inherent in 5 km × 5 km area averaging. Our results compare well with recent convection tank experiments of increased aspect ratio (Deardorff and Willis 1985) and AMTEX observations (Lenschow et al. 1980) except near the surface. Our w^2 also compares well with Nicholls and LeMone's (1980) GATE data (not shown here). The results indicate that many of the first- and second-moment statistics from the $(96)^3$ LES are not significantly different from those of the $(40)^3$ simulation. We will show later, however, that the scalar variance in mid-PBL is about 50% larger in the $(96)^3$ simulations.

The higher-order moments are more sensitive to the LES resolution, however. Figure 3 displays the third-order moments $\overline{w^3}/w_*^3$, $\overline{w^2\theta}/(w_*^2\theta_*)$, and

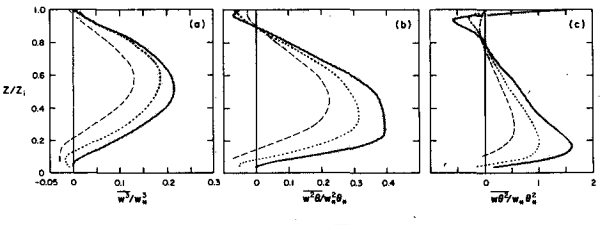

FIG. 3. Vertical distributions of (a) $\overline{w^3}$, (b) $\overline{w^2\theta}$, and (c) $\overline{w\theta^2}$ from the $(40)^3$ LES with a Gaussian filter (dashed curves), the $(96)^3$ LES with a Gaussian filter (dotted curves), and the $(96)^3$ LES with a wave cutoff filter (solid curves).

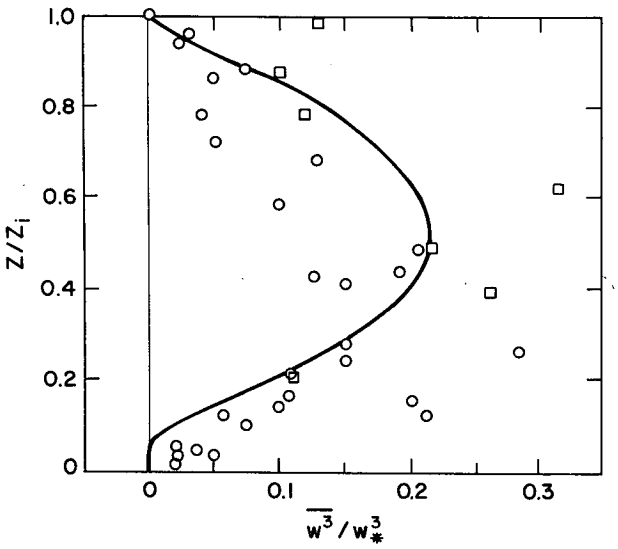

FIG. 4. Vertical distributions of $\overline{w^3}$ from the $(96)^3$ LES (solid curve), convection tank experiments (squares), and AMTEX (circles).

$\overline{w\theta^2}/(w_*\theta_*^2)$ calculated from the resolvable-scale fields from these simulations: (1) $(40)^3$, Gaussian filter; (2) $(96)^3$, Gaussian filter; and (3) $(96)^3$, wave-cutoff filter. Moeng and Wyngaard (1988) explained these different filtering processes. Throughout most of the PBL these third moments from LES are generally larger with finer LES grid resolution and with the wave-cutoff filter. The smaller third moments with the Gaussian filter may be due to (1) its larger filter width (twice the average grid size), and (2) its less sharp transfer function, which causes some attenuation even well below the cutoff frequency (Piomelli et al. 1987; Moeng and Wyngaard 1988). The reduced unrealistic negative $\overline{w^3}/w_*^3$ near the surface in the $(96)^3$ wave-cutoff LES, compared with the other two simulations, implies that the wave-cutoff filter provides more reasonable higher-moment statistics. Their improved spectral distribution studied by Moeng and Wyngaard (1988) also supports the use of a wave-cutoff filter.

We compare $\overline{w^3}/w_*^3$ from our $(96)^3$ wave-cutoff filtered LES with data from AMTEX (Lenschow et al. 1980) and from the tank experiments (Deardorff and Willis 1985) in Fig. 4; the LES result agrees well with the observations and tank experiments throughout most of the PBL. Near the surface our $\overline{w^3}/w_*^3$ is slightly smaller than the AMTEX data; the subgrid-scale contribution may account for the difference (Hunt et al. 1988). The comparison of $\overline{w^2\theta}$ and $\overline{w\theta^2}$ between our LES and observations will be made in section 4.

Figure 5 shows the kinetic energy budget for the resolvable-scale velocity field from the $(96)^3$ LES. All but the dissipation term were computed directly; ϵ was taken as the residual. Figure 5b shows that our turbulent transport and dissipation terms compare well with data from AMTEX and from the convection tank experiments. The pressure transport term also agrees with the convection-tank result, which Deardorff and Willis deduced from the imbalance of the measured terms (Fig. 5c). Pressure transport represents a loss in mid-PBL and shows clear indications of being a substantial source in the surface layer, as inferred from the 1968 Kansas experiments (Wyngaard et al. 1971).

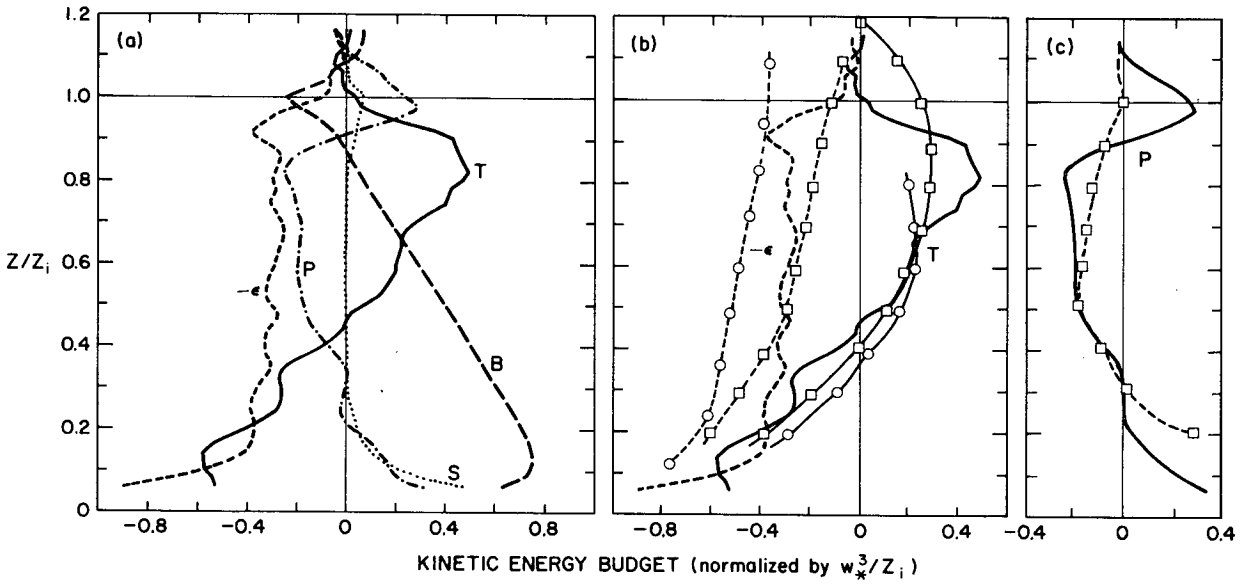

FIG. 5. The kinetic energy budget from the $(96)^3$ LES and comparisons of the turbulent transport, dissipation, and pressure transport terms with results from the convection tank (squares) and AMTEX (circles). T, S, B, P, and ϵ approximately represent the terms on the right side of (2.1).

The only significant difference between our results and the tank experiment appears at the PBL top. There the LES budget shows a gain due to pressure transport, compensating the losses to buoyancy and dissipation, but the tank experiment shows a gain by turbulent transport to compensate the loss. It is not clear what causes this difference, but our interfacial layer Richardson number, $\beta g z_i \Delta\Theta / w_*^2$ (where $\Delta\Theta$ is the inversion strength), is larger than the tank value by a factor of 2–3.

Shear production is negligibly small above the surface layer, so that these LES runs are not suitable for studying the physics of momentum transport.

Figure 6 shows the resolvable-scale buoyancy flux budget. In this case all terms were directly obtained from the LES data; the residual is nearly zero, since the subgrid-scale diffusion is small in this fine-resolution LES. Turbulent transport is as important as the buoyancy and pressure terms in mid-PBL. The mean-gradient term changes sign in mid-PBL where the buoyancy flux is positive; thus, the eddy-diffusivity assumption for the buoyancy flux becomes invalid there. This is consistent with Deardorff's (1966) early analysis of the countergradient heat flux in the convective PBL.

The temperature-variance budget is given in Fig. 7. We computed the transport and mean-gradient production from the LES data. Representing the subgrid-scale diffusivity by K, the subgrid-scale contribution is

$$2\overline{\theta \frac{\partial}{\partial x_i}\left(K \frac{\partial \theta}{\partial x_i}\right)} = 2 \frac{\partial}{\partial x_i} \overline{K \frac{\partial \theta}{\partial x_i} \theta} - 2\overline{K\left(\frac{\partial \theta}{\partial x_i}\right)^2}, \quad (3.1)$$

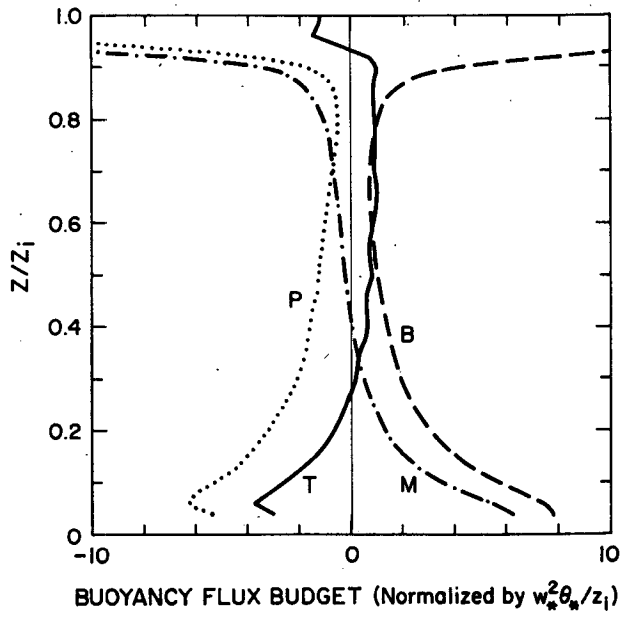

FIG. 6. The buoyancy flux budget from the $(96)^3$ LES data. T, M, B, and P approximately represent the terms on the right side of (2.4) with $c = \theta$.

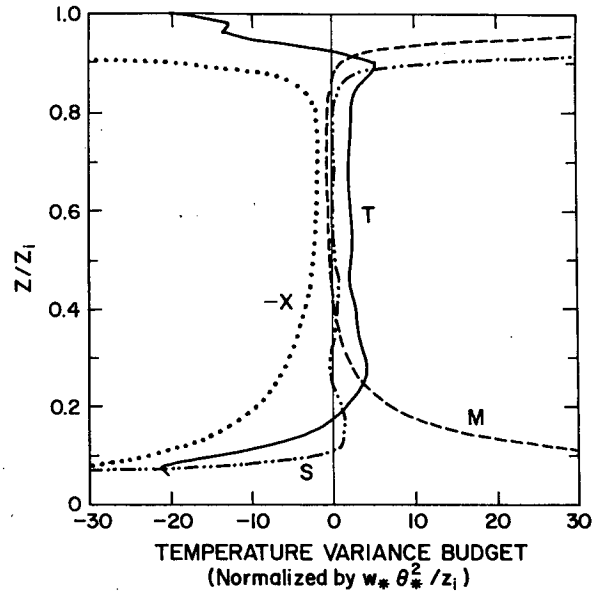

FIG. 7. The temperature variance budget from the $(96)^3$ LES data. T and M represent the turbulent transport and mean-gradient production; χ and S represent the dissipative and diffusive parts of the subgrid-scale term. T, M, and χ approximately represent terms on the right side of (2.5) with $c = \theta$.

the sum of diffusion and dissipation. We computed the dissipation (χ) using the subgrid-scale eddy diffusivity from the LES data, and took the diffusion (S) to be the budget imbalance. The mean-gradient production term is actually a loss in mid-PBL due to the countergradient temperature flux, but it is much smaller in magnitude than turbulent transport there. Thus, to a good approximation the mid-PBL temperature variance budget is a balance between gain by turbulent transport from below and loss to molecular destruction.

4. Evaluation of second-order closures

a. Closures for turbulent energy transport

Figure 8 shows good agreement among dimensionless energy fluxes $\overline{wq^2}/2w_*^3$ computed from our LES data and measured in a convection tank (Deardorff and Willis 1985) and in the convective PBL (Lenschow et al. 1980). Thus, let us use the LES data to examine the eddy-diffusion parameterization (2.2) for turbulence kinetic energy transport. We define an eddy diffusivity K_e for the energy flux as

$$K_e = -\overline{wq^2/2} \Big/ \left(\frac{\partial \overline{q^2}/2}{\partial z}\right). \quad (4.1)$$

In evaluating (4.1) with the LES data we smoothed $\partial(\overline{q^2}/2)/\partial z$. Figure 9 shows the resulting K_e profile from our LES data, and a closure used by Mellor and Yamada (1974), $K_e^{MY} = 0.38 Lq$ with L given by

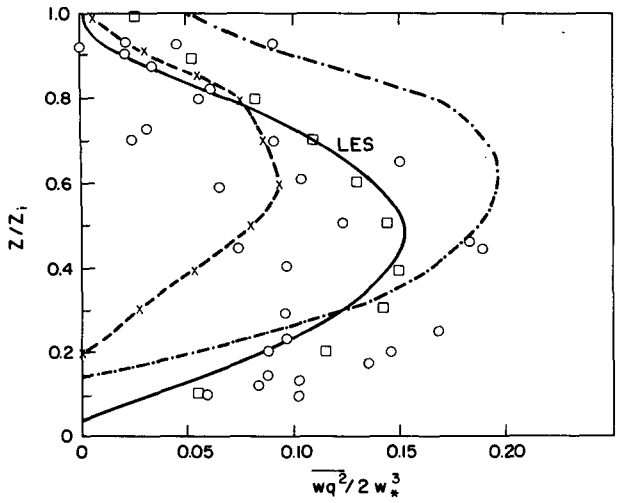

FIG. 8. The vertical flux of energy from the $(96)^3$ LES (solid curve) compared with the parameterizations of Zeman and Lumley (dash-dot curve), Sun and Ogura (dash-cross curve), the convection tank experiment (squares), and AMTEX (circles).

(2.10). The results show that the eddy diffusivity obtained from this closure are much smaller than implied by the LES results, so that the energy flux $\overline{wq^2}/2$ is substantially underpredicted by Mellor and Yamada's closure.

However, the Mellor–Yamada eddy diffusivity does not seem small; its maximum value, about $0.02w_*z_i$ in mid-PBL, is of the order of the $0.05w_*z_i$ estimated by Wyngaard (1983) for the eddy diffusivity of momentum in the baroclinic, convective boundary layer. Rather, the diffusivity of order $1.0w_*z_i$ implied by the LES results seems unphysically large. We also computed the eddy diffusivity for the total transport (turbulent plus pressure); it is also of the order of $1.0w_*z_i$ and positive throughout most of the PBL except near the surface.

We can gain some insight into this issue from the $\overline{wq^2}$ budget. Hanjalic and Launder (1972) used this equation to develop a closure for turbulence–kinetic-energy transport in shear flow, Lumley et al. (1978) used it in their buoyant transport model, and Brost et al. (1980) used it for the stratus-topped PBL. The budget of $\overline{wq^2}/2$ in a horizontally homogeneous boundary layer is

$$\frac{\partial \overline{wq^2}/2}{\partial t} = -\overline{uw^2}\frac{\partial U}{\partial z} - \overline{vw^2}\frac{\partial V}{\partial z} + \overline{uw}\frac{\partial \overline{uw}}{\partial z} + \overline{vw}\frac{\partial \overline{vw}}{\partial z} + \overline{w^2}\frac{\partial \overline{w^2}}{\partial z} + \frac{\overline{q^2}}{2}\frac{\partial \overline{w^2}}{\partial z} - \frac{1}{2}\frac{\partial \overline{w^2q^2}}{\partial z} + \beta g\left(\frac{\overline{q^2\theta}}{2} + \overline{w^2\theta}\right) + P + M. \quad (4.2)$$

Here P and M represent the pressure and molecular terms, whose specific roles here are not entirely clear. However, for third-moment budgets in general, there is evidence that such terms can be quite important. For example, the budget of $\overline{\theta^3}$ in the convective boundary layer is balanced by molecular destruction (Wyngaard and Sundararajan 1979); the sum of the pressure and molecular terms in the budget for $\overline{w^2c}$ in homogeneous turbulence is a strong loss term (Deardorff 1978); and the sum of the pressure and molecular terms in the budget of $\overline{w^3}$ in the unstable surface layer is a net gain (Wyngaard 1980).

If we apply the quasi-normal approximation to the fourth-moment term, (4.2) becomes

$$\frac{\partial \overline{wq^2}/2}{\partial t} = -\overline{uw^2}\frac{\partial U}{\partial z} - \overline{vw^2}\frac{\partial V}{\partial z} \quad \text{(a)}$$

$$-\overline{uw}\frac{\partial \overline{uw}}{\partial z} - \overline{vw}\frac{\partial \overline{vw}}{\partial z} \quad \text{(b)}$$

$$-\frac{\overline{w^2}}{2}\frac{\partial \overline{q^2}}{\partial z} \quad \text{(c)}$$

$$-\overline{w^2}\frac{\partial \overline{w^2}}{\partial z} \quad \text{(d)}$$

$$+\beta g\left(\frac{\overline{q^2\theta}}{2} + \overline{w^2\theta}\right) \quad \text{(e)}$$

$$+P + M. \quad \text{(f)}$$

(4.3)

The terms on the right-hand side of (4.3) represent the effects of (a) the mean shear, (b) the stress gradient,

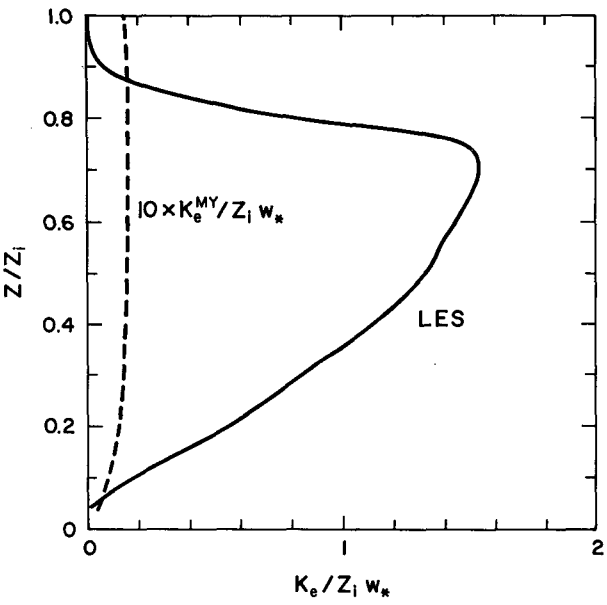

FIG. 9. Profiles of the eddy diffusivity for energy flux, defined in (4.1), from the $(96)^3$ LES (solid curve) and that implied by Mellor and Yamada's parameterization (dashed curve). The latter is magnified by a factor of ten.

(c) the $\overline{q^2}$ gradient, (d) the $\overline{w^2}$ gradient, (e) buoyancy, and (f) pressure and molecular diffusivity. In the convective boundary layer terms (a) and (b) are normally much smaller than the rest, so we will not consider them further. A comparison of terms (c), (d), and (e), Fig. 10, indicates that (e) (buoyancy) is the largest, and that (d) (the $\overline{w^2}$-gradient term) is also generally larger in magnitude than (c), the $\overline{q^2}$-gradient term.

If term (f) is of order $-\overline{wq^2}/\tau$, where τ is a time scale (Hanjalic and Launder 1972; Lumley 1975), then (4.3) shows that the conventional downgradient closure (2.2) applied to the convective boundary layer is equivalent to ignoring the dominance of the $\overline{w^2}$-gradient and buoyancy and writing under stationary conditions

$$\frac{\overline{w^2}}{2}\frac{\partial \overline{q^2}}{\partial z} = P + M \sim -\frac{\overline{wq^2}}{\tau} \Rightarrow \overline{wq^2} \sim -\overline{w^2}\tau\frac{\partial \overline{q^2}}{\partial z}. \tag{4.4}$$

In parameterizing the turbulent transport as (4.4), however, we are forced to use an unrealistically large value of K_e (i.e., $\overline{w^2}\tau$) in order to achieve the LES-observed ratio of $\overline{wq^2}$ and $-\partial\overline{q^2}/\partial z$, as shown by Fig. 9. In other words, the presence of the dominant terms (d) and (e) in (4.3) not proportional to $\partial\overline{q^2}/\partial z$ means that a downgradient diffusion closure for $\overline{wq^2}$ is not appropriate.

In modeling turbulent transport in the convective boundary layer, it is therefore necessary to include buoyancy effects. Zeman and Lumley (1976) and Lumley et al. (1978) carried diagnostic equations for third-moment quantities. Their model thus explicitly includes the buoyancy effects on third moments, but since buoyancy makes the third moments interdependent no simple flux-gradient relationship of the form of (4.4) exists. Figure 8 indicates that Zeman and Lumley's model predicts $\overline{wq^2}$ behavior that agrees fairly well with the observational and LES data. Using Zeman and Lumley's buoyancy transport closure in the Mellor-Yamada model, Sun and Ogura (1980) improved the energy flux somewhat, as also shown in Fig. 8. In their eddy-kinetic-energy model, Therry and Lacarrére (1983) also modified the downgradient-flux formulation by using a simple empirical closure, derived from a third-order closure model, for the buoyancy term.

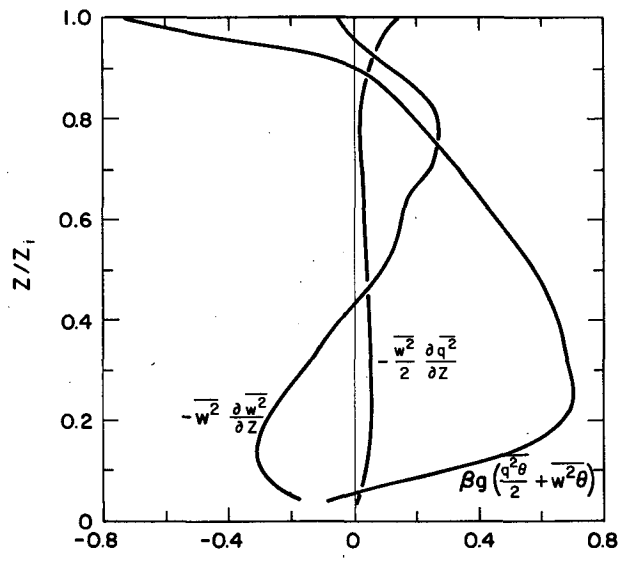

FIG. 10. Profiles of terms (c), (d), and (e) in the $\overline{wq^2}/2$ budget (4.3) from the $(96)^3$ LES.

b. Closures for scalar-flux and -variance transports

1) TOP-DOWN, BOTTOM-UP DECOMPOSITION

We can get some insight into the gradient-diffusion assumption for scalar transport by representing a conservative scalar field c as the sum of "top-down" and "bottom-up" components, a technique applied by Wyngaard and Brost (1984) and Moeng and Wyngaard (1984). Thus, if $c = c_t + c_b$, we write $\overline{w^2c}$ as

$$\overline{w^2c} = \overline{w^2c_t} + \overline{w^2c_b}. \tag{4.5}$$

Similarly, we write $\overline{wc^2}$ as

$$\overline{wc^2} = \overline{wc_t^2} + \overline{wc_b^2} + 2\overline{wc_tc_b}. \tag{4.6}$$

We now examine the adequacy of the usual second-order closure for these third moments, which we write as

$$\overline{w^2c_t} = -K_t^{(f)}\frac{\partial \overline{wc_t}}{\partial z}, \tag{4.7a}$$

$$\overline{w^2c_b} = -K_b^{(f)}\frac{\partial \overline{wc_b}}{\partial z}, \tag{4.7b}$$

and

$$\overline{wc_t^2} = -K_t^{(v)}\frac{\partial \overline{c_t^2}}{\partial z}, \tag{4.8a}$$

$$\overline{wc_b^2} = -K_b^{(v)}\frac{\partial \overline{c_b^2}}{\partial z}, \tag{4.8b}$$

$$\overline{wc_tc_b} = -K_{tb}^{(v)}\frac{\partial \overline{c_tc_b}}{\partial z}. \tag{4.8c}$$

The superscripts (f) and (v) on K refer to the scalar flux and scalar-scalar covariance, respectively. We write the K's as the product of length and velocity scales,

$$K_t^{(f)} = L_t^{(f)}q, \quad K_b^{(f)} = L_b^{(f)}q, \tag{4.9}$$

and

$$K_t^{(v)} = L_t^{(v)}q, \quad K_b^{(v)} = L_b^{(v)}q, \quad K_{tb}^{(v)} = L_{tb}^{(v)}q. \tag{4.10}$$

We included three passive, conservative scalars in our large-eddy simulation; one represents top-down diffusion, while the other two have both surface- and entrainment-induced fluxes and therefore represent the

general case with combined top-down and bottom-up diffusion. Using the technique described in Moeng and Wyngaard (1984), we retrieved the bottom-up, top-down, and joint statistics from these three scalar fields. We compare the gradient functions g_t and g_b from our $(40)^3$ and $(96)^3$ simulations in Fig. 11. They are defined by

$$\frac{\partial C_t}{\partial z} = -\frac{\overline{cw}_1}{w_* z_i} g_t \qquad (4.11a)$$

$$\frac{\partial C_b}{\partial z} = -\frac{\overline{cw}_0}{w_* z_i} g_b, \qquad (4.11b)$$

where $\overline{cw}_1$ is the flux of c at the top of the mixed layer and $\overline{cw}_0$ the flux of c at the surface. The difference between the $(96)^3$ and $(40)^3$ results is generally not large, but does tend to increase the dissimilarity of the top-down and bottom-up functions. Figure 12 shows the variance functions f_t, f_b, and f_{tb}, defined by

$$\overline{c_t^2} = \left(\frac{\overline{cw}_1}{w_*}\right)^2 f_t, \qquad (4.12a)$$

$$\overline{c_b^2} = \left(\frac{\overline{cw}_0}{w_*}\right)^2 f_b, \qquad (4.12b)$$

$$\overline{c_t c_b} = \frac{\overline{cw}_1 \overline{cw}_0}{w_*^2} f_{tb}, \qquad (4.12c)$$

$$\overline{c^2} = \overline{c_t^2} + \overline{c_b^2} + 2\overline{c_t c_b}. \qquad (4.12d)$$

The top-down and bottom-up variance functions f_t and f_b are somewhat larger than those found by Moeng and Wyngaard (1984) with a $(40)^3$ grid. Since the computed variances include only the resolvable-scale contribution, this reflects the increased resolution of the $(96)^3$ LES. In Fig. 12 we also give new curve fits to f_t and f_b based on the $(96)^3$ LES.

Although the covariance function f_{tb} is also larger than in the $(40)^3$ simulation, its scaled value $\gamma = f_{tb}/(f_t f_b)^{1/2}$ remained about the same, 0.5, in the mixed layer. One can show from (4.12) that the correlation coefficient between the c_b and c_t fields, $r = \overline{c_t c_b}/$

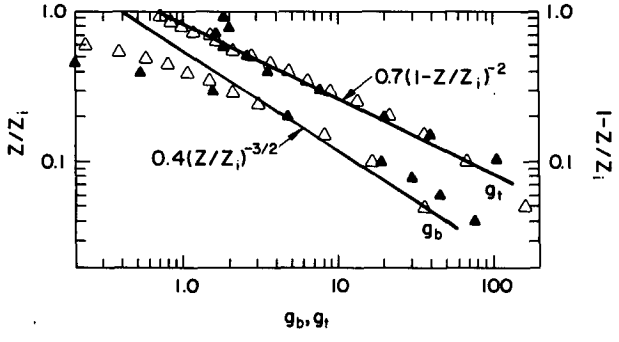

FIG. 11. The top-down and bottom-up gradient functions from the $(40)^3$ LES (open triangles) and the $(96)^3$ LES (solid triangles), and the curve fits of Moeng and Wyngaard (1984).

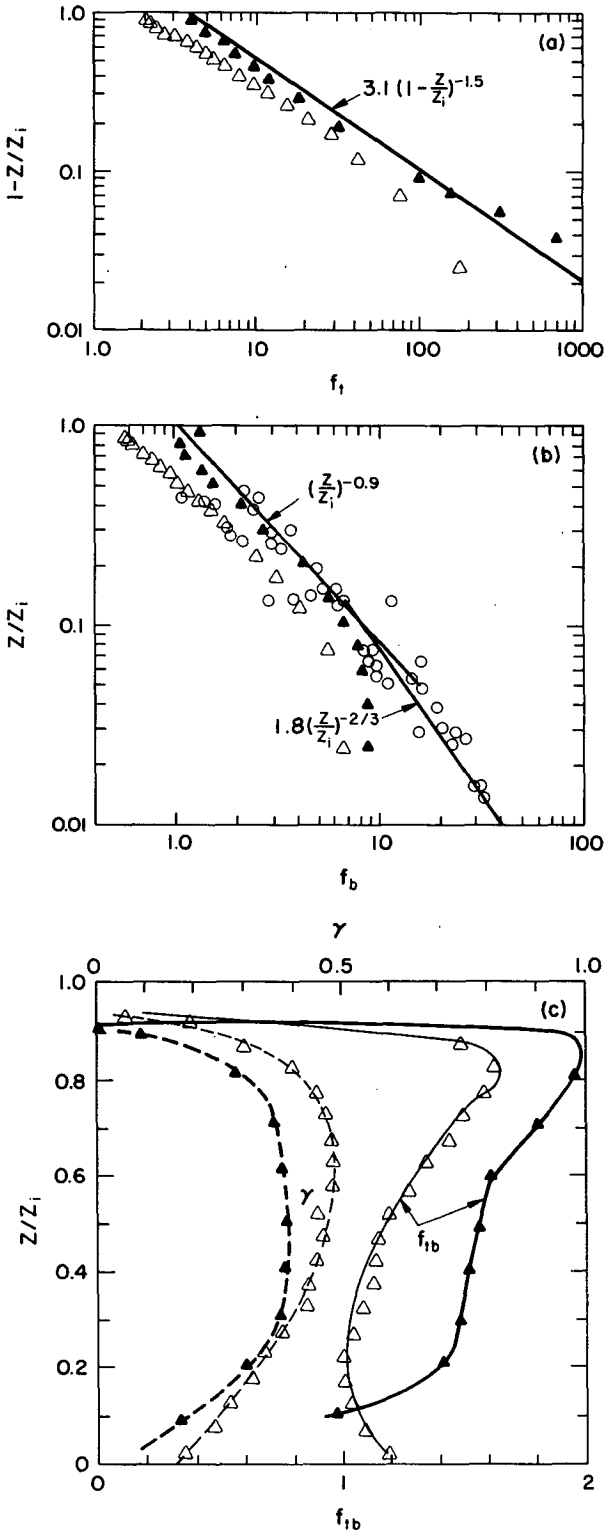

FIG. 12. The variance functions of (a) a top-down scalar, (b) a bottom-up scalar, and (c) the covariance function between top-down and bottom-up scalars; the data are from the $(40)^3$ LES (open triangles) and the $(96)^3$ LES (solid triangles). The solid curves are new curve fits based on the $(96)^3$ results, and based on surface layer observations for the curve fit of f_b below 0.1 z_i. Open circles are the Minnesota data.

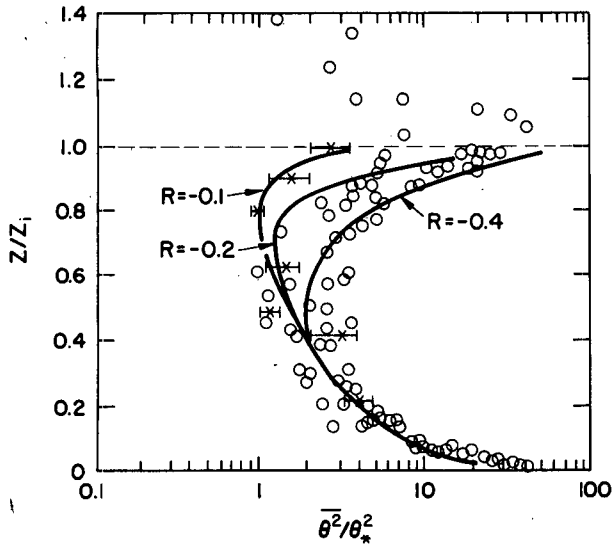

FIG. 13. The temperature variance computed from (4.12) using the curve fits shown in Fig. 12. R is the ratio of entrainment and surface fluxes. Circles, AMTEX data; X, convection tank data.

$(\overline{c_t^2 c_b^2})^{1/2}$ has magnitude γ; since f_{tb} is positive, the sign of r is the sign of the product of $\overline{cw_0}$ and $\overline{cw_1}$. It follows that if, for example, $\overline{cw_0}$ is positive (i.e., there is an upward flux of c_b through the surface) and $\overline{cw_1}$ is negative (a downward entrainment flux of c_t) then within the mixed layer $r \sim -0.5$. This suggests the coexistence of positive c_b fluctuations and negative c_t fluctuations in updrafts under these conditions. The substantial correlation between c_t and c_b means that in general the cross-correlation contribution to the total variance, Eq. (4.12d), is not negligible.

Our calculation of the temperature variance profile, using (4.12) and the variance functions from the $(96)^3$ simulations, is shown in Fig. 13. It is about 50% larger than the profile from the $(40)^3$ results and also agrees better with atmospheric data. It agrees particularly well with the Deardorff–Willis (1985) convection tank results.

We show the LES results for the components of $\overline{w^2 c}$ and $\overline{wc^2}$ in Fig. 14. Here the cross component, $\overline{wc_t c_b}$, is quite small in the mixed layer and we will neglect it. (The sudden sign change of $\overline{wc_t^2}$ near the top is probably spurious and due to the finite-difference error resulting from the sharp gradient of the top-down scalar.) We used these data to compute the length scales $L_t^{(\downarrow)}$, $L_b^{(\downarrow)}$, $L_t^{(\uparrow)}$, and $L_b^{(\uparrow)}$ in (4.7)–(4.10), shown in Fig. 15. We used linear profiles of scalar flux; i.e., $\overline{c_t w} = \overline{cw}_1 z/z_i$ and $\overline{c_b w} = \overline{cw}_0(1 - z/z_i)$ in (4.7). We used the analytical curve fits for the variance functions in (4.8) in order to facilitate the z-differentiation.

The results in Fig. 15b indicate that the length scale (and the eddy diffusivity) for bottom-up variance is larger than for the top-down variance. This is also the case for the more familiar eddy diffusivity for scalar flux (Wyngaard and Brost 1984). Figure 15a shows that $L_t^{(\downarrow)}$, and, hence, the eddy diffusivity for $w^2 c_t$, is negative, meaning that a downgradient diffusion assumption is inappropriate here. We can interpret this negative eddy diffusivity physically as follows. Consider the top-down diffusion of a scalar introduced from

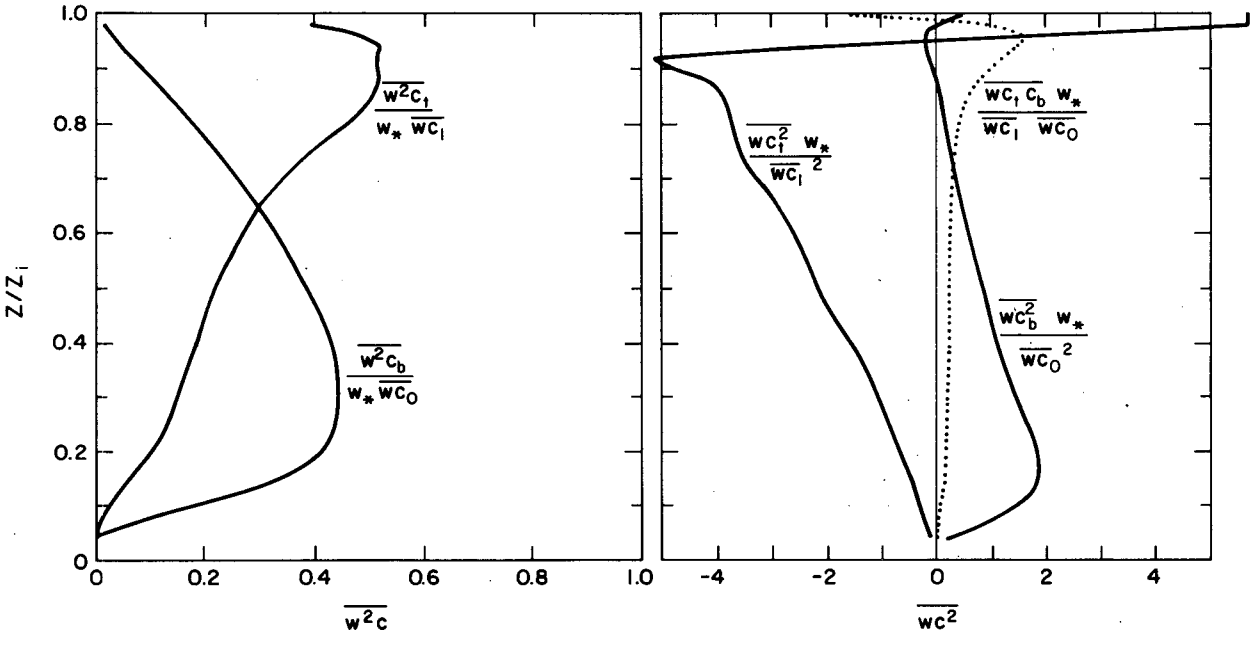

FIG. 14. The top-down, bottom-up, and joint contributions to $\overline{w^2 c}$ and $\overline{wc^2}$.

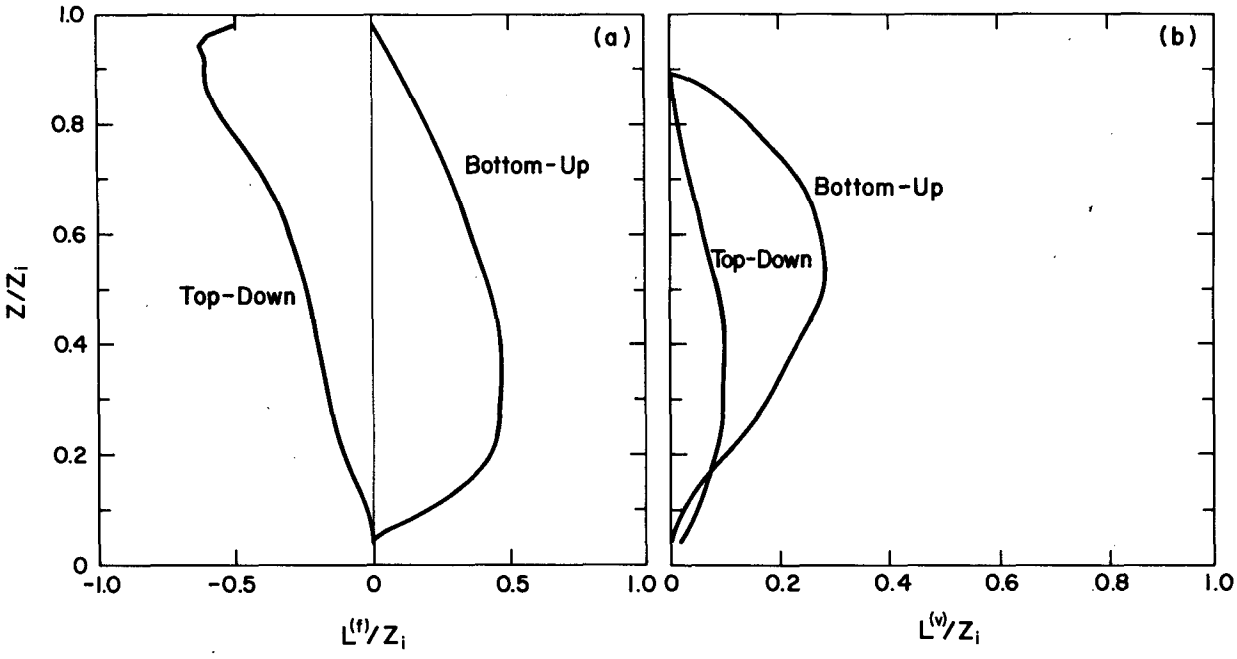

FIG. 15. The downgradient-diffusion length scales, defined in (4.7)–(4.10), for (a) $\overline{w^2c}$ and (b) $\overline{wc^2}$.

above, say, so that $\overline{wc_t}$ and $\partial\overline{wc_t}/\partial z$ are negative. Both updrafts with low scalar concentrations and downdrafts with high concentrations contribute to the negative value of $\overline{wc_t}$. Since the w-field is positively skewed, however, the updraft processes make the dominant contributions to $\overline{w^2c_t}$ and cause it to be negative, so that its eddy diffusivity is also negative. This is consistent with both potential temperature (θ) and humidity (m) observations from AMTEX (Lenschow et al. 1980), as we will show in section 4.b.3.

Next, we will analyze the budgets of $\overline{wc_t^2}$, $\overline{wc_b^2}$, $\overline{w^2c_t}$, and $\overline{w^2c_b}$ to get more insight into the applicability of the gradient-diffusion assumption for each.

2) BUDGETS OF $\overline{wc_t^2}$, $\overline{wc_b^2}$, $\overline{w^2c_t}$, AND $\overline{w^2c_b}$

The budget of $\overline{w^2c}$ is

$$\frac{\partial\overline{w^2c}}{\partial t} = -\overline{w^3}\frac{\partial C}{\partial z} + 2\overline{wc}\frac{\partial\overline{w^2}}{\partial z} + \overline{w^2}\frac{\partial\overline{wc}}{\partial z} - \frac{\partial\overline{w^3c}}{\partial z} + 2\beta g\overline{w\theta c} - 2\frac{1}{\rho_0}\overline{wc\frac{\partial p}{\partial z}} + M. \quad (4.13)$$

Here M represents the molecular terms, which are diffusive and possibly also dissipative. If we drop the time-rate-of-change term, apply the quasi-normal approximation to the fourth-moment term, and assume that the sum of the pressure and molecular terms is proportional to $-\overline{w^2c}/\tau$, where $\tau \sim L/q$ is an energy-containing-range time scale (e.g., André et al. 1982), (4.13) becomes

$$\overline{w^2c} = -\frac{L}{q}\left(\underbrace{\overline{w^3}\frac{\partial C}{\partial z}}_{(a)} + \underbrace{2\overline{w^2}\frac{\partial\overline{wc}}{\partial z}}_{(b)} + \underbrace{\overline{wc}\frac{\partial\overline{w^2}}{\partial z}}_{(c)} - \underbrace{2\beta g\overline{w\theta c}}_{(d)}\right). \quad (4.14)$$

The terms on the right side of (4.14) represent the effects of (a) the mean gradient, (b) the flux gradient, (c) the $\overline{w^2}$ gradient, and (d) buoyancy.

We compare these four terms (normalized by w_*, $\overline{wc_1}$, and z_i) for the top-down case in Fig. 16a. We plot only the quantities inside the bracket on (4.14); thus, negatives are source terms for the normalized $\overline{w^2c}$ and positives are sinks. The conventional downgradient-diffusion assumption (4.7a) is equivalent to retaining only the flux-gradient effect, term (b) on the right side of (4.14). Figure 16a shows that (b) is actually one of the smaller terms in the budget, and that retaining only it gives a negative length scale and negative eddy diffusivity). The mean-gradient term is much larger than the flux-gradient term and together with the buoyancy term accounts for the sign of $\overline{w^2c_t}$.

The budget of the bottom-up component, $\overline{w^2c_b}$, is shown in Fig. 16b after normalization by w_*, $\overline{wc_0}$, and z_i. Both the flux-gradient and buoyancy terms are sources (which are shown as negative in the figure) throughout the PBL. This explains why the downgradient diffusion approximation gives a positive length scale. However, Fig. 16b shows that the buoyancy effect

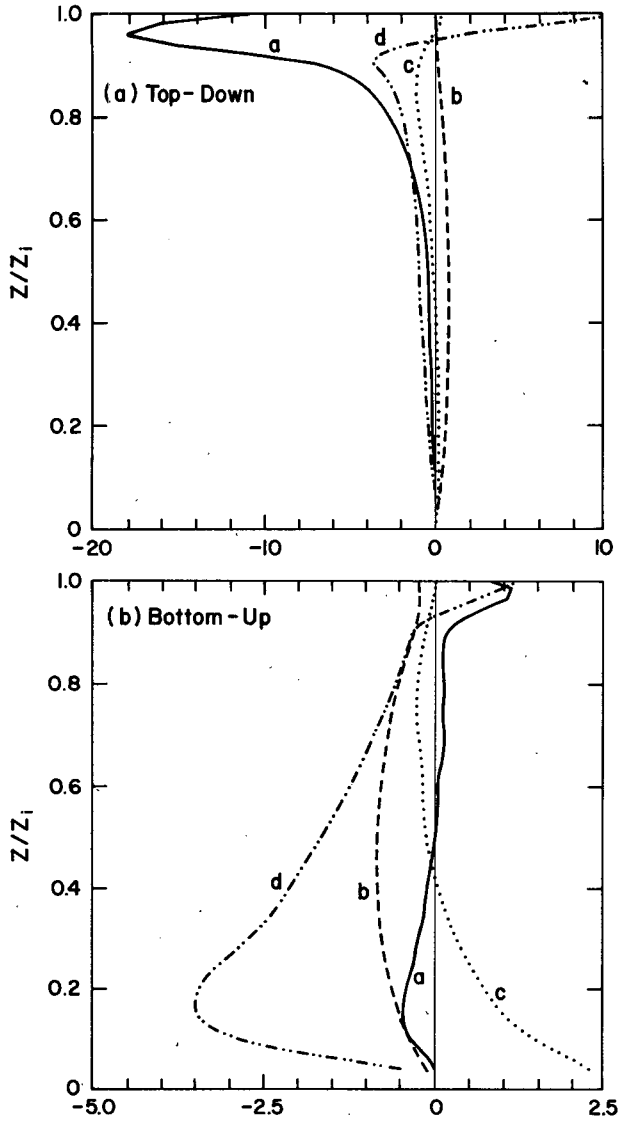

FIG. 16. The mean-gradient (labeled a), flux-gradient (b), $\overline{w^2}$-gradient (c), and buoyancy (d) terms in the $\overline{w^2c}$ budgets (4.14) for top-down and bottom-up cases.

dominates, which also explains why downgradient transport models with a length scale L adjusted for neutral flows greatly underestimate the transport.

The budget for $\overline{wc^2}$ is

$$\frac{\partial \overline{wc^2}}{\partial t} = -2\overline{w^2c}\,\frac{\partial C}{\partial z} + 2\overline{wc}\,\frac{\partial \overline{wc}}{\partial z} + \overline{c^2}\,\frac{\partial \overline{w^2}}{\partial z} - \frac{\partial \overline{w^2c^2}}{\partial z} + \beta g\overline{\theta c^2} - 2\,\frac{1}{\rho_0}\,\overline{c^2\,\frac{\partial p}{\partial z}} + M_2, \quad (4.15)$$

where M_2 represents the molecular terms. Applying the quasi-normal approximation to the fourth-moment term, assuming that the sum of the pressure and molecular terms is proportional to $-\overline{wc^2}/(L/q)$, and dropping the time-rate-of-change term gives

$$\overline{wc^2} = -\frac{L}{q}\left(\underbrace{2\overline{w^2c}\,\frac{\partial C}{\partial z}}_{\text{(a)}} + \underbrace{\overline{w^2}\,\frac{\partial \overline{c^2}}{\partial z}}_{\text{(b)}} + \underbrace{2\overline{wc}\,\frac{\partial \overline{wc}}{\partial z}}_{\text{(c)}} - \underbrace{\beta g\overline{\theta c^2}}_{\text{(d)}}\right). \quad (4.16)$$

The normalized top-down results are shown in Fig. 17a. Term (b) is larger than the others by at least a factor of 2 and is a sink (shown in the figure as positive) for negative wc_t^2; thus, L defined by retaining only term (b) in (4.16) is positive.

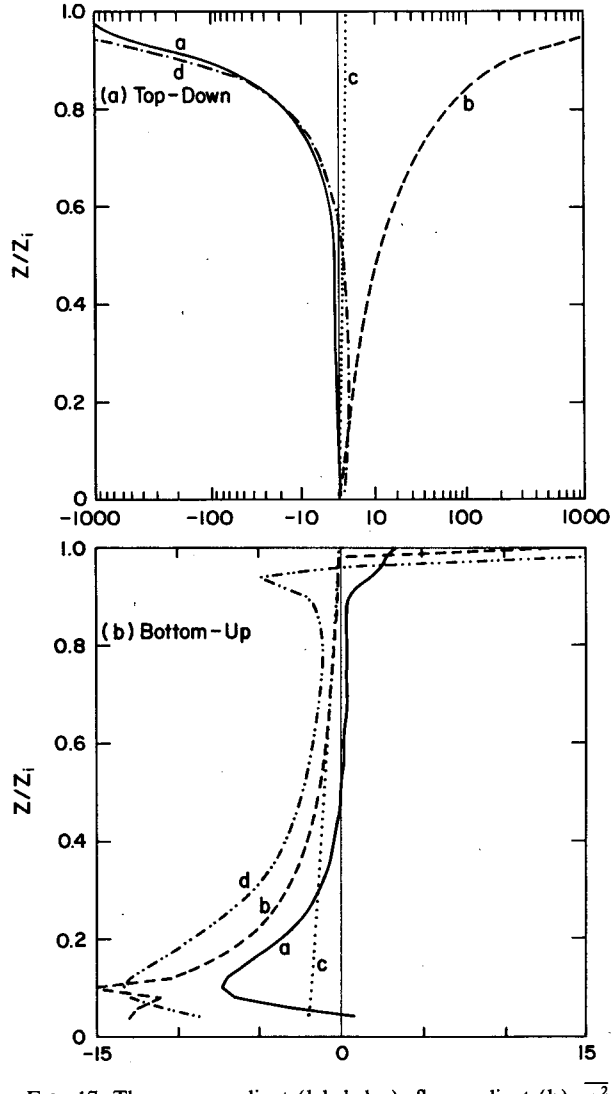

FIG. 17. The mean-gradient (labeled a), flux-gradient (b), $\overline{w^2}$-gradient (c), and buoyancy (d) terms in the $\overline{wc^2}$ budgets (4.16) for top-down and bottom-up cases. The abscissa in Fig. 17a is a linear-logarithmic scale transformation of $y = (x/|x|)\ln(1 + |x|/x_0)$.

The normalized budget for $\overline{wc_b^2}$ is given in Fig. 17b. In the lower half of the PBL all four terms are sources; hence, retaining only the variance-gradient term (b) [as used in (4.8b)] leads to a positive length scale, as shown in Fig. 15.

3) Comparison with observations

In Fig. 18 we compare our predictions of $\overline{w^2\theta}$ and $\overline{w\theta^2}$, calculated from the top-down and bottom-up results given in Fig. 14, with direct measurements from AMTEX (Lenschow et al. 1980) and Minnesota (Kaimal et al. 1976). Our calculation assumes $\overline{\theta w}_1/\overline{\theta w}_0 = -0.2$. The large scatter of the observations, probably due in part to the inadequate averaging time (Wyngaard 1973), indicates the great difficulty in using direct PBL measurements for studying closures. There is also a suggestion of a systematic difference between the two sets of measurements and indications of the predicted sign change of both $\overline{w^2\theta}$ and $\overline{w\theta^2}$ near the PBL top due to entrainment effects.

For the moisture field we assumed the entrainment-surface moisture flux ratio $\overline{wm}_1/\overline{wm}_0 = 0.5$ and 1, as typically observed in AMTEX (Lenschow et al. 1980) and GATE (Nicholls and LeMone 1980). Figure 19 compares the predicted $\overline{w^2m}$ and $\overline{wm^2}$ with data obtained from AMTEX and GATE (M. A. LeMone 1988, personal communication). The GATE data have an entrainment-surface flux ratio of about 1, while the AMTEX data have a ratio of about 0.5; thus, we predict the GATE data to have larger dimensionless $\overline{w^2m}$ in the upper PBL, and the results are consistent with this. We also predict the dimensionless $\overline{wm^2}$ data from GATE to have the larger negative values near PBL top, shown in Fig. 19, although for unknown reasons the AMTEX data fail to show any negative values.

4) Evaluation of currently used closures

Mellor and Yamada (1974) use the parameterizations

$$\overline{w^2\theta} = -0.23qL\frac{\partial\overline{w\theta}}{\partial z} \tag{4.17}$$

and

$$\overline{w\theta^2} = -0.23qL\frac{\partial\overline{\theta^2}}{\partial z}, \tag{4.18}$$

where L is calculated from (2.10) with constants adjusted for neutral flows. Figure 20 shows that these closures greatly underestimate $\overline{w^2\theta}$ and $\overline{w\theta^2}$, simply because they neglect the dominant effects of buoyancy.

The model of Zeman and Lumley (1976), which includes buoyancy but neglects the mean gradient terms in (4.14) and (4.16), gives $\overline{w^2\theta}$ and $\overline{w\theta^2}$ in good agreement with our LES data, as also shown in Fig. 20. This is consistent with the dominance of buoyancy effects in the $\overline{w^2c_b}$ and $\overline{wc_b^2}$ budgets. It remains to be seen whether their model can predict the profile of $\overline{w^2m}$, which has a significant top-down component and thus a dominant mean-gradient effect in the upper PBL. Sun and Ogura (1980) modified the Mellor-Yamada model to incorporate Zeman and Lumley's buoyancy transport closure; this yields some improve-

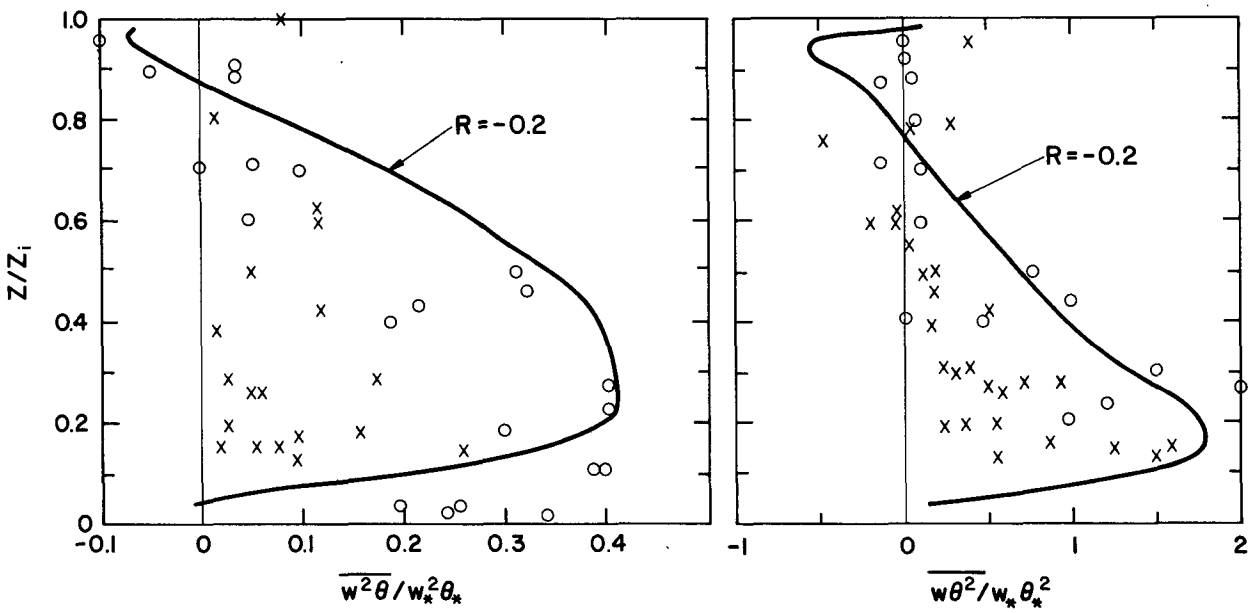

FIG. 18. Comparisons of $\overline{w^2\theta}$ and $\overline{w\theta^2}$ computed from our results for top-down and bottom-up cases (solid curves) with the Minnesota data (crosses) and the AMTEX data (circles).

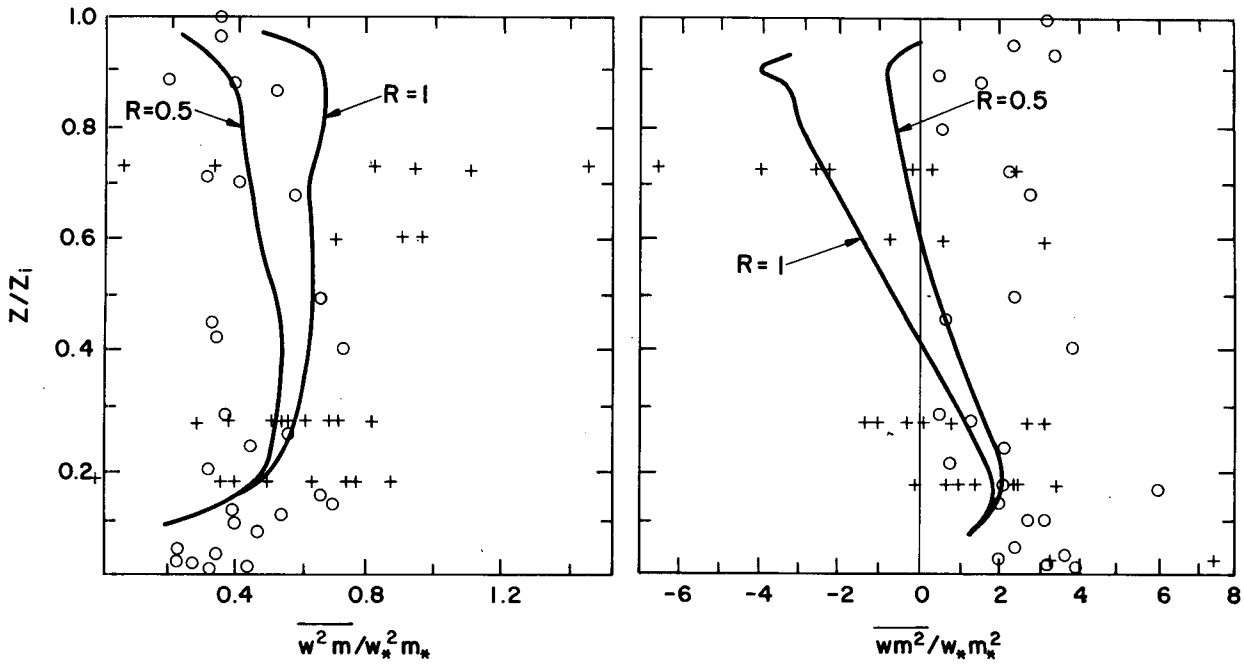

FIG. 19. Comparisons of $\overline{w^2 m}$ and $\overline{wm^2}$ computed from our results for top-down and bottom-up cases (solid curves) with the GATE data (crosses, courtesy of M. A. LeMone) and the AMTEX data (circles).

ment over the Mellor-Yamada model in predicting these third-moment quantities, according to Fig. 20. Sun and Ogura's model differs from Zeman and Lumley's mainly in the length (or time) scale used for computing these fluxes; their length scale is smaller than that of Zeman and Lumley, as we will show in sections 4.c and d.

c. *Closures for mechanical dissipation rate*

Using the LES data on $\overline{q^2}/2$ and ϵ in Figs. 1 and 5, we calculated the dissipation length scale $L_2 = q^3/\epsilon$. Figure 21 compares the results with the often used (e.g., Mellor and Yamada 1974; Sun and Ogura 1980) closure $L_2 = 15L$, with L from (2.10). The LES results

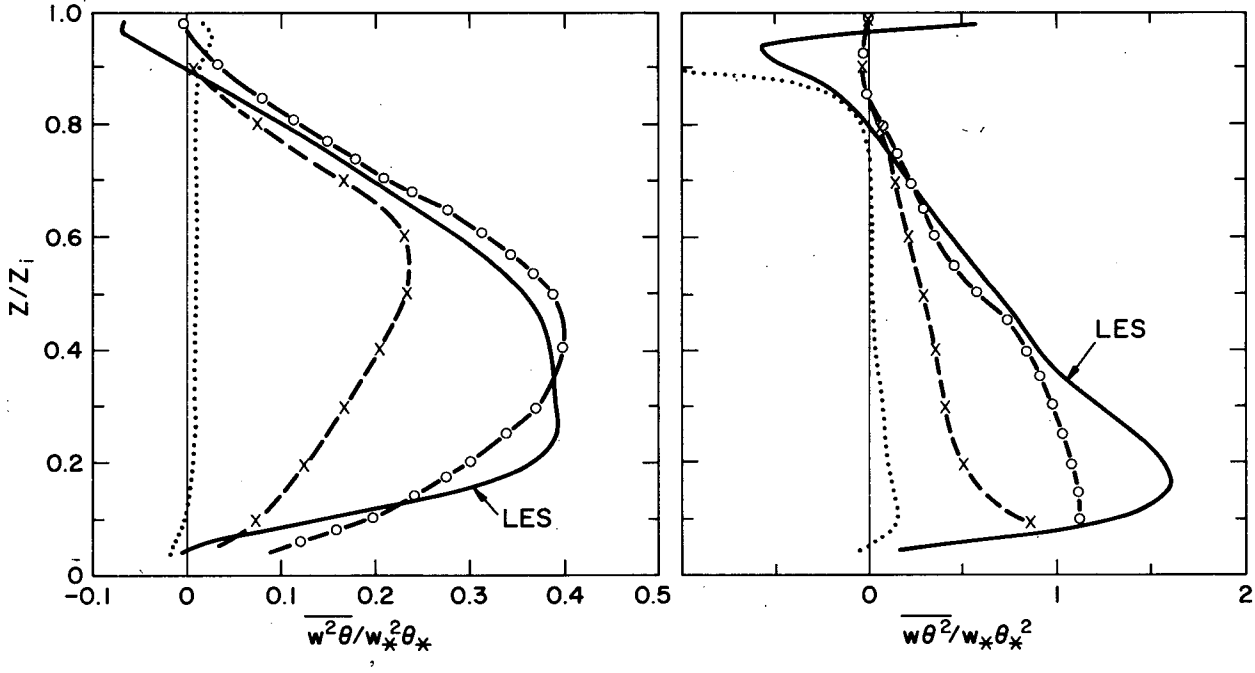

FIG. 20. The profiles of $\overline{w^2\theta}$ and $\overline{w\theta^2}$ from the $(96)^3$ LES (solid curves) compared with the parameterizations of Zeman and Lumley (dash-circle curves), Sun and Ogura (dash-cross curves), and Mellor and Yamada (dotted curves).

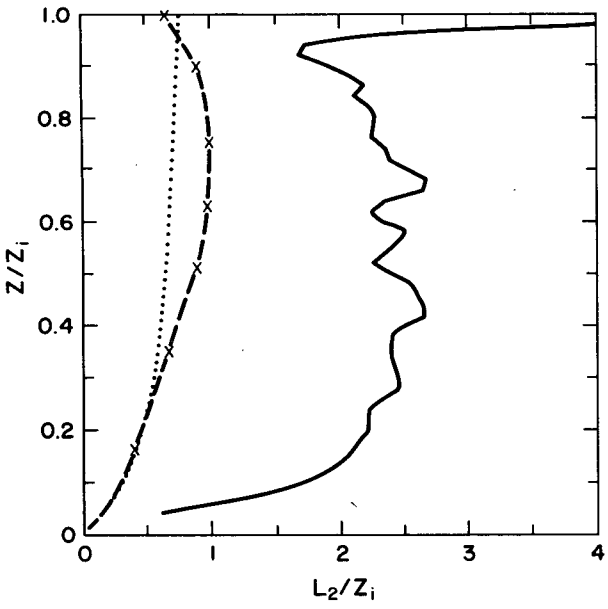

FIG. 21. Characteristic length scale for dissipation rate obtained from our $(96)^3$ LES kinetic-energy budget (solid curve) compared with the closures of Mellor and Yamada (dotted curve), and Sun and Ogura (dash-cross curve).

indicate that $L_2 \approx 2.5z_i$ in mid-PBL, about 3 times the value given by this closure.

In their third-order closure model, André et al. (1978) used a dissipation length scale which is comparable to our value. They parameterized dissipation rate as $0.07(\overline{q^2}/2)^{3/2}/L$ with L from (2.10). Since $(\overline{q^2}/2)^{3/2} \approx 0.35q^3$, this is equivalent to adopting a length scale $L_2 = L/(0.35 \times 0.07)$, about three times larger than that of Mellor and Yamada; this is more consistent with our results. This agreement with André et al. (1978) is not surprising, since they determined their empirical constant for the dissipation rate from Deardorff's (1974) LES data for the convective boundary layer. Therry and Lacarrére (1983) and Chen and Cotton (1983) also used the André et al. dissipation parameterization.

More recently, Mellor and Yamada (1982) suggested using a prognostic equation for q^2L, and their results suggest a larger value of $\alpha_b = 0.2$ (rather than 0.1) in (2.11) (Mellor 1989, personal communication).

Since $\overline{q^2}/2 \approx 0.4w_*^2$ in the mid-PBL, the LES produces the time scale $\tau \equiv L_2/q \approx 2.8z_i/w_*$ in mid-PBL. This agrees well with observations of $\overline{q^2}/\epsilon$ by Isaka and Guillemet (1983). The integral scale $2.5z_i$ is about the size of the largest wave resolvable in our LES model; this may suggest that a horizontal domain of 5 km × 5 km is marginal for resolving the largest turbulent eddies.

d. Closures for scalar-variance dissipation rate

We show the dissipation time scale τ, defined as

$$\tau = -\frac{\overline{c^2}}{\chi_c}, \tag{4.19}$$

in Fig. 22. The dissipation time scale for top-down variance is on the order of $1.0z_i/w_*$, about the same as that from our $(40)^3$ simulation (Moeng and Wyngaard 1984). The time scale for bottom-up variance, however, is smaller by about 50% compared with the previous $(40)^3$ simulation. This increases the dissimilarity of the top-down and bottom-up fields.

The length scale L_6 used to model the molecular destruction rate of scalar variance, χ_c, is usually assumed to be proportional to that used for ϵ. Equations (2.3) and (2.9) give us the ratio of these two length scales,

$$\frac{L_6}{L_2} = \frac{\overline{c^2}\epsilon}{\overline{q^2}\chi_c}. \tag{4.20}$$

We evaluated the right-hand side of (4.20) for potential temperature and for the top-down and bottom-up scalar fields. The results shown in Fig. 23 indicate that L_6 for the top-down variance is about a factor of 2 larger than for the bottom-up variance in mid-PBL. This length scale for the top-down component decreases with height while that for the bottom-up one stays constant.

The ratio L_6/L_2 computed from the potential temperature field is smaller everywhere than that for the bottom-up scalar. This is apparently due to the contribution from the correlation of the top-down and bottom-up fields. Figure 24 compares L_6/L_2 retrieved from the top-down and bottom-up fields for different entrainment-surface flux ratios. The profile for $R = -0.2$ agrees well with that from the potential temperature field.

To first approximation, in mid-PBL $L_6/L_2 \approx 0.2$ for the bottom-up variance and ≈ 0.4 for the top-down

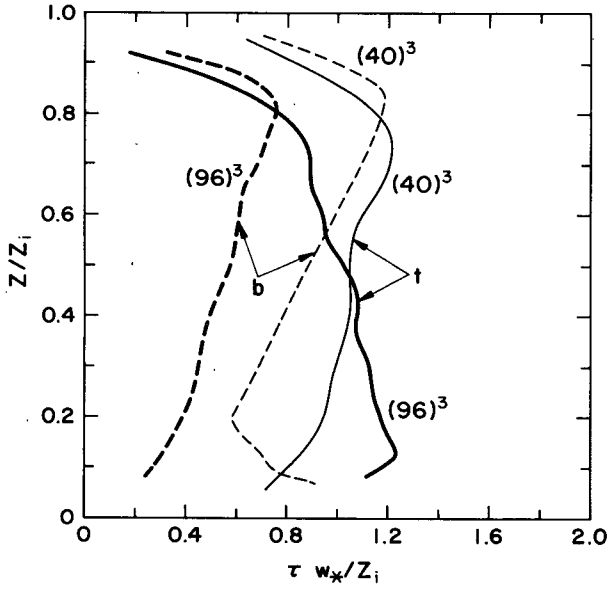

FIG. 22. The dissipation time scales of top-down (solid curves) and bottom-up (dashed curves) scalar fields from our $(40)^3$ and $(96)^3$ LES.

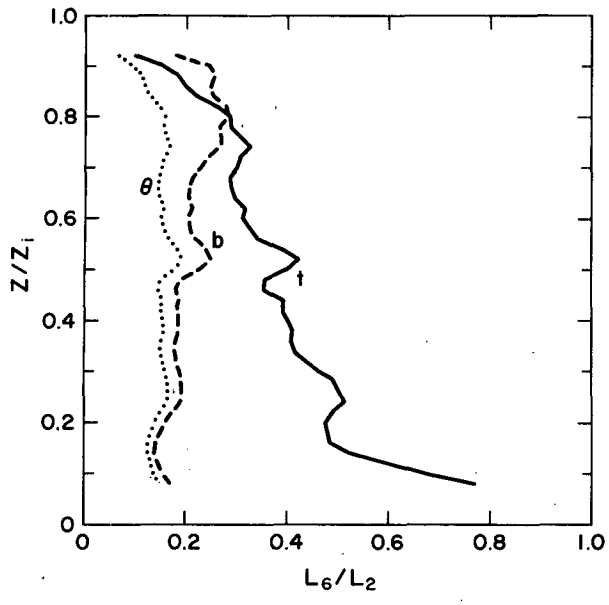

FIG. 23. Ratio of the scalar-variance dissipation length scale to the mechanical dissipation length scale computed from (4.20); χ_c from the variance budgets of a top-down scalar (solid curve), a bottom-up scalar (dashed curve), and potential temperature (dotted curve).

variance. Based on a large collection of data from the convective boundary layer, Isaka and Guillemet (1983) reported that

$$\frac{\overline{\theta^2}\epsilon}{\overline{q^2}\chi_\theta} = 0.19, \quad \frac{\overline{m^2}\epsilon}{\overline{q^2}\chi_m} = 0.28, \qquad (4.21)$$

where m is water vapor mixing ratio. Their value of $L_6/L_2 = 0.19$ for temperature agrees well with our value of ~0.2; their value of $L_6/L_2 = 0.28$ for water vapor lies between our bottom-up and top-down values, consistent with the observation that water vapor typically has positive fluxes at PBL top and bottom. For a scalar field with an equal amount of entrainment and surface fluxes, Fig. 24 predicts that $L_6/L_2 = 0.36$. Mellor and Yamada (1982) used $L_6/L_2 \approx 0.3[B_2/(2B_1)$ in their notation], which falls within the range of our results. Since their L_2 seems small by a factor of 3, their L_6 may also be small by that factor.

5. Implications for second-order closure models

Because a second-order closure model is a complicated, nonlinear system with feedback, its response to parameterization changes can be difficult to predict. However, we can make some broad statements about the effects of the parameterization errors we have discussed.

a. Velocity statistics

The buoyant production rate, the principal source of turbulence in the convective boundary layer, is proportional to the vertical flux of temperature $\overline{w\theta}$. If the mean lapse rate $\partial\Theta/\partial z$ is independent of time, the $\overline{w\theta}$ profile is linear because its second derivative vanishes:

$$\frac{\partial}{\partial t}\frac{\partial\Theta}{\partial z} = 0 = -\frac{\partial^2}{\partial z^2}\overline{w\theta}. \qquad (5.1)$$

Most observational and model studies show that in the absence of abrupt changes in boundary conditions, the $\overline{w\theta}$ profile is indeed essentially linear in the mixed layer, with some curvature appearing near the capping inversion layer.

Thus, given the proper boundary conditions, second-order models will tend to have the correct vertical profile of buoyant production rate within the mixed layer, regardless of the fidelity of their closure parameterizations. If we integrate the turbulence kinetic energy equation (2.1) across the convective PBL, neglecting the shear production term, we find, to a good approximation, under steady conditions

$$\int_0^{h_2} \epsilon(z)dz \approx \beta g \int_0^{h_2} \overline{w\theta}(z)dz \approx 0.4\beta g\overline{w\theta}_0, \qquad (5.2)$$

where h_2 is the turbulent layer top. The constant 0.4 results from assuming that $\overline{w\theta}_1 = -0.2\overline{w\theta}_0$. Closure approximations can affect the $\overline{w\theta}$ profile near the mixed-layer top, but the overall effect is simply to vary the constant in (5.2) over the the range 0.4 to about 0.5. Thus, we conclude that the layer-integrated ϵ value is nearly independent of closure approximations. This is illustrated in Fig. 25, which compares ϵ profiles from the LES and those from the second-order models of Zeman and Lumley (1976), Sun and Ogura (1980), and Yamada and Mellor (1975). For the latter, we use

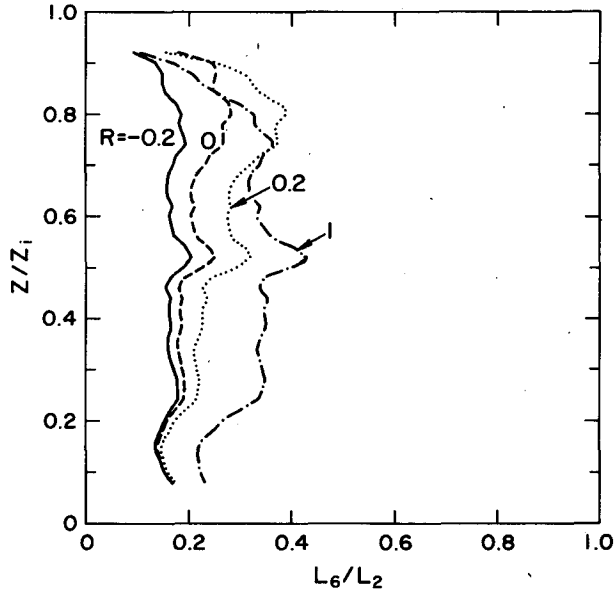

FIG. 24. Ratio of the scalar-variance dissipation length scale to the mechanical dissipation length scale predicted from the top-down and bottom-up results and varying entrainment-surface flux ratio.

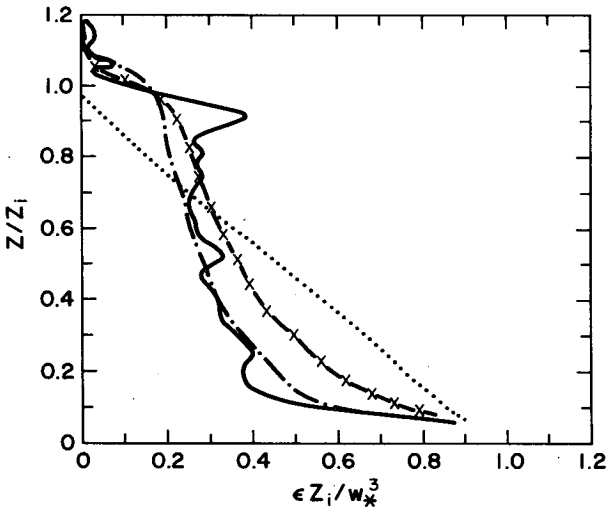

FIG. 25. The dissipation rate from our $(96)^3$ LES (solid curve) compared with the model predictions of Zeman and Lumley (dash-dot curve), Sun and Ogura (dash-cross curve), and Yamada and Mellor (dotted curve).

z_i = 1100 m and w_* = 2.2 m s^{-1} with a surface buoyancy flux 0.3 m K s^{-1} obtained by linearly extrapolating the mid-layer buoyant production profile in their turbulence kinetic energy budget. Each integrates over the PBL to roughly the same value, despite the fact that the Mellor and Yamada model uses a dissipation length scale that is small by a factor of 3.

Because of incorrect turbulent and pressure transport parameterizations, however, the errors in the *local* energy budget in the Mellor and Yamada model can be substantial, as suggested in Fig. 25. This error also causes the entrainment flux $w\theta_1$ to be underestimated, which in turn increases the constant in (5.2) to about 0.5 and increases the layer-averaged dissipation rate by 25%.

If a second-order closure model uses a parameterization of the form $\epsilon = q^3/L_2$, then since ϵ is essentially fixed incorrect prescriptions of the length scale L_2 will result in incorrect q^2 values. This is illustrated in Fig. 26, which compares q^2 values from Yamada and Mellor (1975) and the LES. Our arguments predict that the error in their length scale gives the layer-integrated q^2 values small by a factor of $3^{2/3} \approx 2$, in good agreement with Fig. 26. Finger and Schmidt (1986) used α_b = 0.2 in the Mellor–Yamada model and predicted much reasonable vertical energy levels.

b. *Scalar statistics*

1) MOLECULAR DISSIPATION

If we integrate the scalar variance budget (2.5) over the boundary layer we find, in steady conditions,

$$-2\int_0^{h_2} \overline{wc}\,\frac{\partial C}{\partial z}\,dz = \int_0^{h_2} \chi_c dz. \qquad (5.3)$$

While as we stated the vertical profile of $\overline{wc}$ is independent of closure parameterizations, $\partial C/\partial z$ is determined principally by the $\overline{wc}$ equation; as a result, it is sensitive to the closure. Thus, from (5.3) the layer-integrated value of χ_c from a closure model, unlike the layer-integrated ϵ, depends on the closure.

We can separate the first integral in (5.3) into two parts, the first over the surface and mixed layers and the second over the interfacial layer, defined as the region of negative entrainment flux of temperature near the PBL top (Deardorff 1979). $\Delta h = h_2 - h_0$, where h_2 and h_0 are the top and bottom of the interfacial layer. The interfacial layer integral is, from the results of Wyngaard and LeMone (1980),

$$-2\int_{h_0}^{h_2} \overline{wc}\,\frac{\partial C}{\partial z}\,dz \approx \int_{h_0}^{h_2} \chi_c dz \approx 1.4\,\frac{(\Delta C)^2 w_* \Delta h}{z_i\,\mathrm{Ri}}, \qquad (5.4)$$

where $\mathrm{Ri} = \beta g z_i \Delta\Theta / w_*^2$ is the interfacial layer Richardson number defined in Section 3 and $\Delta C = C(h_2) - C(h_0)$. Thus, χ_c near the boundary-layer top depends on Ri. In the case of temperature (5.4) is (Wyngaard and LeMone 1980)

$$\int_{h_0}^{h_2} \chi_\theta dz \approx \frac{2\,\mathrm{Ri}\theta_*^2 w_* \Delta h}{15 z_i}, \qquad (5.5)$$

which again contains Ri. This Ri dependence complicates comparisons of model predictions, since it is not one of the usual mixed-layer scaling parameters.

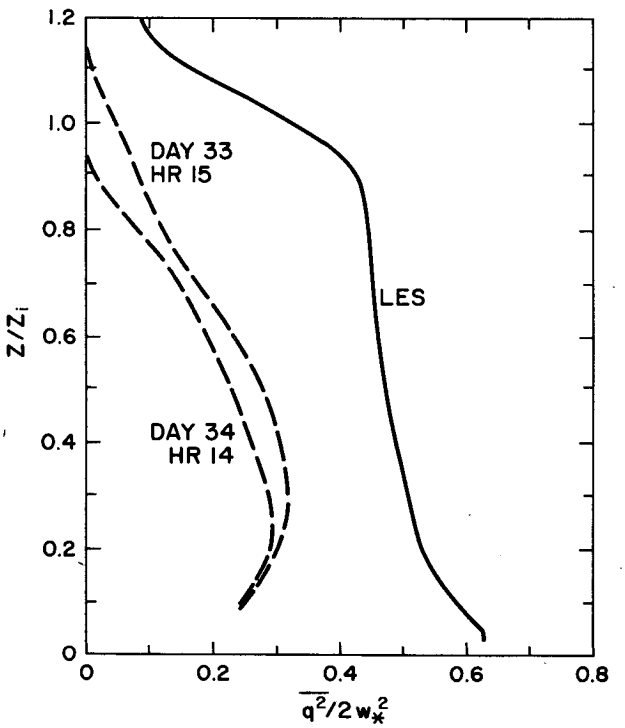

FIG. 26. The kinetic energy from our $(96)^3$ LES compared with the model predictions of Yamada and Mellor (dashed curves).

Nonetheless, in low- to mid-PBL the χ_θ values of Sun and Ogura (1980) and Yamada and Mellor (1975) compare well with our LES results. The details of their $\overline{\theta^2}$ budgets do not agree as well; however; both models underpredict the turbulent transport term which, as we show in Fig. 7, essentially balances χ_θ in mid-PBL. The downgradient-diffusion closure in Mellor and Yamada's model results in (a) no sign change of $\partial\Theta/\partial z$ in mid-layer and (b) a significant underestimate of χ_θ, hence the temperature structure parameter C_T^2, in upper regions of the PBL (Fairall 1987).

2. TOP-DOWN/BOTTOM-UP ASYMMETRY

There are substantial differences between the scalar flux budgets in top-down and bottom-up diffusion. In this study we showed that the transport terms behave quite differently in the two cases. The bottom-up third moment w^2c_b behaves as in gradient diffusion (i.e., it is down the gradient of $\overline{wc_b}$), while w^2c_t is upgradient. Thus, a single parameterization for scalar flux transport (as used in most second-order models) does not capture the differences in transport in the bottom-up and top-down cases.

Earlier we pointed out analogous differences in the pressure covariances (Moeng and Wyngaard 1986). The pressure covariance in the scalar flux equation is often parameterized as

$$\overline{c\frac{\partial p}{\partial z}} = \frac{\overline{wc}}{T}, \tag{5.6}$$

where T is an energy-containing-range time scale. We found that T is substantially different for top-down and bottom-up processes. We also decomposed the turbulent kinematic pressure field into components representing turbulence-turbulence interactions, mean shear, buoyancy, Coriolis forces, and subgrid-scale effects:

$$p = p_T + p_S + p_B + p_C + p_{SG}. \tag{5.7}$$

Using Rotta's parameterization for the turbulence-turbulence part of pressure gives

$$\overline{c\frac{\partial p_T}{\partial z}} = \frac{\overline{wc}}{\tau}, \tag{5.8}$$

and we found that the time scale τ was different in the top-down and bottom-up cases.

If we assume that two different top-down fields are well correlated, and that two different bottom-up fields are also well correlated, then we can write

$$\theta = \theta_t + \theta_b \approx \frac{\overline{w\theta_1}}{\overline{wc_1}}c_t + \frac{\overline{w\theta_0}}{\overline{wc_0}}c_b \tag{5.9}$$

(Moeng and Wyngaard 1984). Thus, the buoyant production term in the scalar flux budget (2.4) for the top-down and bottom-up cases becomes

$$\beta g\overline{c_t\theta} \approx \left(\beta g\frac{\overline{w\theta_1}}{\overline{wc_1}}\right)\overline{c_t^2} + \left(\beta g\frac{\overline{w\theta_0}}{\overline{wc_0}}\right)\overline{c_tc_b}, \tag{5.10a}$$

and

$$\beta g\overline{c_b\theta} \approx \left(\beta g\frac{\overline{w\theta_0}}{\overline{wc_0}}\right)\overline{c_b^2} + \left(\beta g\frac{\overline{w\theta_1}}{\overline{wc_1}}\right)\overline{c_tc_b}, \tag{5.10b}$$

respectively. Since we showed earlier that the variance functions of c_t^2 and c_b^2 are different, we conclude from (5.10) that the buoyant production terms in the scalar flux budgets also differ in bottom-up and top-down cases.

It follows that since the turbulent transport, pressure covariance, and buoyant production terms all differ in the top-down and bottom-up scalar flux budgets in the convective boundary layer, the usual second-order closures for these budgets are not uniformly valid for an arbitrary scalar flux profile; i.e., second-order closures for, say, temperature and moisture flux budgets should be different. Contrary to the assertion of Lewellen et al. (1985), the asymmetry in top-down and bottom-up diffusion is not due to the presence of turbulent transport, but to the different physics of diffusion in the two cases. This seems to be a result of the skewed vertical velocity field and could be a general property of diffusion in skewed turbulence.

3) CORRECTIONS TO THE FLUX-GRADIENT RELATIONSHIP

A simplified version of second-order closure modeling carries only the turbulence kinetic energy equation and relates heat and momentum fluxes to mean gradients through eddy diffusivities. As mentioned in sections 2 and 3, this eddy-diffusivity assumption can be invalid because of countergradient diffusion. Some models (e.g., Mailhot and Benoit 1982; Therry and Lacarrére, 1983), following Deardorff (1972), try to compensate in the case of temperature through a correction term γ_θ:

$$\overline{w\theta} = -K_h\left(\frac{\partial\Theta}{\partial z} - \gamma_\theta\right), \tag{5.11}$$

where $K_h \propto \tau\overline{w^2}$ and $\gamma_\theta = \beta g\overline{\theta^2}/\overline{w^2}$. Deardorff derived this formula from (2.4) by ignoring turbulent transport and using the Rotta closure (2.8) on the pressure covariance. This formula has two discrepancies for the convective PBL because (a) the turbulent transport is important, as shown in Fig. 6, and (b) a buoyancy correction is needed for the pressure-covariance term (Moeng and Wyngaard 1986).

Nevertheless, if a closure model uses (5.11), for consistency it should use a similar formula for other scalar fluxes, such as moisture flux:

$$\overline{wc} = -K_h\left(\frac{\partial C}{\partial z} - \gamma_c\right), \tag{5.12}$$

where $\gamma_c = \beta g\overline{\theta c}/\overline{w^2}$. From (5.10) and Figs. 2 and 12 we can estimate γ_c for any scalar. It should vary with the entrainment-surface flux ratio, however.

Acknowledgments. We thank the reviewers, Peggy LeMone, and Don Lenschow for their comments on the manuscript, and Fran Huth for editing it.

REFERENCES

André, J. C., G. De Moor, P. Lacarrere and R. Du Vachat, 1976: Turbulence approximation for inhomogeneous flows. Part 1: The clipping approximation. *J. Atmos. Sci.*, **33,** 476–481.

——, ——, ——, G. Therry and R. Du Vachat, 1978: Modeling the 24-hour evolution of the mean and turbulent structures of the planetary boundary layer. *J. Atmos. Sci.*, **35,** 1861–1883.

——, P. Lacarrere and K. Traoré, 1982: Pressure effects on triple correlations in turbulent convective flows. *Turbulent Shear Flows,* Springer-Verlag, 243–252.

Blackadar, A. K., 1962: The vertical distribution of wind and turbulent exchange in a neutral atmosphere. *J. Geophys. Res.*, **67,** 3095–3102.

Brost, R. A., and J. C. Wyngaard, 1978: A model study of the stably stratified planetary boundary layer. *J. Atmos. Sci.*, **35,** 1427–1440.

——, —— and D. H. Lenschow, 1980: Marine stratocumulus layers. Part II: Turbulence budgets. *J. Atmos. Sci.*, **39,** 818–836.

Burk, S. D., 1977: The moist boundary layer with a higher order turbulence closure model. *J. Atmos. Sci.*, **34,** 629–638.

Chen, C., and W. R. Cotton, 1983: A one-dimensional simulation of the stratoculumus-capped mixed layer. *Bound. Layer Meteor.*, **25,** 289–321.

Deardorff, J. W., 1966: The counter-gradient heat flux in the lower atmosphere and in the laboratory. *J. Atmos. Sci.*, **23,** 503–506.

——, 1972: Theoretical expression for the countergradient vertical heat flux. *J. Geophys. Res.*, **77,** 5900–5904.

——, 1974: Three-dimensional numerical study of turbulence in an entraining mixed layer. *Bound. Layer Meteor.*, **7,** 199–226.

——, 1978: Closure of second- and third-moment rate equations for diffusion in homogeneous turbulence. *Phys. Fluids,* **21,** 525–530.

———, 1979: Prediction of convective mixed-layer entrainment for realistic capping inversion structure. *J. Atmos. Sci.*, **36,** 424–436.

——, and G. E. Willis, 1985: Further results from a laboratory model of the convective planetary boundary layer. *Bound. Layer Meteor.*, **32,** 205–236.

Donaldson, C. duP. 1973: Construction of a dynamic model of the production of atmospheric turbulence and the dispersal of atmospheric pollutants. *Workshop on Micrometeorology,* D. A. Haugen, Ed., Amer. Meteor. Soc., 313–390.

Duynkerke, P. G., and A. G. M. Driedonks, 1987: A model for the turbulent structure of the stratocumulus-topped atmospheric boundary layer. *J. Atmos. Sci.*, **44,** 43–64.

Fairall, C. W., 1987: A top-down and bottom-up diffusion model of C_T^2 and C_Q^2 in the entraining convective boundary layer. *J. Atmos. Sci.*, **44,** 1009–1017.

Finger, J. E., and H. Schmidt, 1986: On the efficiency of higher order turbulence models simulating the convective boundary layer. *Beitr. Phys. Atmos.*, **59,** 505–517.

Hanjalic, K., and B. E. Launder, 1972: A Reynolds stress model of turbulence and its application to thin shear flows. *J. Fluid Mech.*, **52,** 609–638.

Helfand, H. M., and J. C. Labraga, 1988: Design of a nonsingular level 2.5 second-order closure model for the prediction of atmospheric turbulence. *J. Atmos. Sci.*, **45,** 113–132.

Hunt, J. C. R., J. C. Kaimal and J. E. Gaynor, 1988: Eddy structure in the convective boundary layer—New Measurements and new concepts. *Quart. J. Roy. Meteor. Soc.*, **114,** 827–858.

Isaka, H., and B. Guillemet, 1983: Molecular dissipation of turbulent fluctuations in the convective mixed layer. Part II: Height variations of characteristic time scales and experimental test of molecular dissipation models. *Bound. Layer Meteor.*, **27,** 257–279.

Kaimal, J. C., J. C. Wyngaard, D. A. Haugen, O. R. Coté, Y. Izumi, S. J. Caughey and C. J. Readings, 1976: Turbulence structure in the convective boundary layer. *J. Atmos. Sci.*, **33,** 2152–2169.

Klein, P., and M. Coantic, 1981: A numerical study of turbulent processes in the marine upper layer. *J. Phys. Oceanogr.*, **11,** 849–863.

Klemp, J. B., and R. B. Wilhelmson, 1978: The simulation of three-dimensional convective storm dynamics. *J. Atmos. Sci.*, **35,** 1070–1096.

Lenschow, D. H., J. C. Wyngaard and W. T. Pennell, 1980: Mean-field and second-moment budgets in a baroclinic, convective boundary layer. *J. Atmos. Sci.*, **37,** 1313–1326.

Lewellen, W. S., 1977: Use of invariant modeling. *Handbook of Turbulence,* W. Frost and T. H. Moulden, Eds., Plenum, 237–277.

——, and M. E. Teske, 1973: Prediction of the Monin-Obukhov similarity functions from an invariant model of turbulence. *J. Atmos. Sci.*, **30,** 1340–1345.

——, R. I. Sykes and S. F. Parker, 1985: Comments on "Scalar diffusion in the convective boundary layer". *J. Atmos. Sci.*, **42,** 1084–1085.

Lumley, J. L., 1970: Toward a turbulent constitutive relation. *J. Fluid Mech.*, **41,** 413–434.

——, 1975: Introduction. *Lecture Series 76: Prediction Methods for Turbulent Flows,* von Kármán Inst. Fluid Dyn., Rhode-St.-Genése, Belgium.

——, 1978: Computational modeling of turbulent flows. *Adv. Appl. Mech.*, **18,** 123–176.

——, and B. Khajeh-Nouri, 1974: Computational modeling of turbulent transport. *Advances in Geophysics,* Vol. 18A, Academic Press, 169–192.

——, O. Zeman and J. Siess, 1978: The influence of buoyancy on turbulent transport. *J. Fluid Mech.*, **84,** 581–597.

Mailhot, J., and R. Benoit, 1982: A finite-element model of the atmospheric boundary layer suitable for use with numerical weather prediction models. *J. Atmos. Sci.*, **39,** 2249–2266.

Mellor, G. L., 1973: Analytic prediction of the properties of stratified planetary surface layer. *J. Atmos. Sci.*, **30,** 1061–1069.

——, and H. J. Herring, 1973: A survey of the mean turbulent field closure models. *AIAA Journal,* **11,** 590–599.

——, and T. Yamada, 1974: A hierarchy of turbulence closure models for planetary boundary layers. *J. Atmos. Sci.*, **31,** 1791–1806.

——, and P. A. Durbin, 1975: The structure and dynamics of the ocean surface mixed layer. *J. Phys. Oceanogr.*, **5,** 718–728.

——, and T. Yamada, 1982: Development of a turbulence closure model for geophysical fluid problems. *Rev. Geophys. Space Phys.*, **20,** 851–875.

Miyakoda, K., and J. Sirutis, 1977: Comparative integrations of global models with various parameterized processes of subgrid-scale vertical transports: Description of the parameterizations. *Beitr. Phys. Atmos.*, **50,** 445–487.

Moeng, C.-H., and A. Arakawa, 1980: A numerical study of a marine subtropical stratus cloud layer and its stability. *J. Atmos. Sci.*, **37,** 2661–2676.

——, and J. C. Wyngaard, 1984: Statistics of conservative scalars in the convective boundary layer. *J. Atmos. Sci.*, **41,** 3161–3169.

——, and ——, 1986: An analysis of closures for pressure-scalar covariances in the convective boundary layer. *J. Atmos. Sci.*, **43,** 2499–2513.

——, and ——, 1988: Spectral analysis of large-eddy simulations of the convective boundary layer. *J. Atmos. Sci.*, **45,** 3573–3587.

Nicholls, S., and M. A. LeMone, 1980: The fair-weather boundary layer in GATE: The relationship of subcloud layer fluxes and structure to the distribution and enhancement of cumulus clouds. *J. Atmos. Sci.*, **37,** 2051–2067.

Oliver, D. A., W. S. Lewellen and G. G. Williamson, 1978: The interaction between turbulent and radiative transport in the development of fog and low-level stratus. *J. Atmos. Sci.*, **35,** 301–316.

Piomelli, U., P. Moin and J. H. Ferziger, 1987: Model consistency in the large eddy simulation of turbulent channel flows. AIAA Paper No. 87-1446.

Rotta, J. C., 1951: Statistische theorie nichthomogener turbulenz. *Z. Phys.*, **129,** 547–572.

Sun, W.-Y., and Y. Ogura, 1980: Modeling the evolution of the convective planetary boundary layer. *J. Atmos. Sci.*, **37**, 1558–1572.

Tennekes, H., and J. L. Lumley, 1972: *A First Course in Turbulence.* M.I.T. Press, 300 pp.

Therry, G., and P. Lacarrére, 1983: Improving the eddy kinetic energy model for planetary boundary layer description. *Bound. Layer Meteor.*, **25**, 63–88.

Wai, M.-K., 1987: A numerical study of the marine stratocumulus cloud layer. *Bound. Layer Meteor.*, **40**, 241–267.

Wyngaard, J. C., 1973: On surface layer turbulence. *Workshop on Micrometeorology,* D. A. Haugen, Ed., Amer. Meteor. Soc., 101–149.

——, 1975: Modeling the planetary boundary layer—Extension to the stable case. *Bound. Layer Meteor.*, **9**, 441–460.

——, 1980: The atmospheric boundary layer—Modeling and measurements. *Turbulent Shear Flows,* Springer-Verlag, 352–365.

——, 1982: Boundary-layer modeling. *Atmospheric Turbulence and Air Pollution Modelling,* F.T.M. Nieuwstadt and H. Van Dop, Eds., Reidel, 69–106.

——, 1983: The mean wind structure of the baroclinic, convective boundary layer. *Proceedings of the First Sino-American Workshop on Mountain Meteorology,* E. R. Reiter, Z. Baozhen and Q. Yongfu, Eds., Amer. Meteor. Soc., 371–396.

——, and O. R. Coté, 1974: The evolution of a convective planetary boundary-layer—A higher-order-closure model study. *Bound. Layer Meteor.*, 289–308.

——, and A. Sundararajan, 1979: The temperature skewness budget in the lower atmosphere and its implications for turbulence modeling. *Turbulent Shear Flows,* Springer-Verlag, 319–326.

——, and M. A. LeMone, 1980: Behavior of the refractive index structure parameter in the entraining convective boundary layer. *J. Atmos. Sci.*, **37**, 1573–1585.

——, and R. A. Brost, 1984: Top-down and bottom-up diffusion of a scalar in the convective boundary layer. *J. Atmos. Sci.*, **41**, 102–112.

——, O. R. Coté and Y. Izumi, 1971: Local free convection, similarity, and the budgets of shear stress and heat flux. *J. Atmos. Sci.*, **28**, 1171–1182.

Yamada, T., and G. L. Mellor, 1975: A simulation of the Wangara atmospheric boundary layer data. *J. Atmos. Sci.*, **32**, 2309–2329.

Zeman, O., 1981: Progress in the modeling of planetary boundary layers. *Annual Review of Fluid Mechanics,* Vol. 13, Annual Reviews, 253–272.

——, and J. L. Lumley, 1976: Modeling buoyancy driven mixed layers. *J. Atmos. Sci.*, **33**, 1974–1988.